039

CNWRA *A center of excellence in earth sciences and engineering*

A Division of Southwest Research Institute
6220 Culebra Road • San Antonio, Texas, U.S.A. 78228-5166
(210) 522-5160 • Fax (210) 522-5155

February 25, 2000
Contract No. NRC-02-97-009
Account No. 20.01402.471

U.S. Nuclear Regulatory Commission
ATTN: Dr. Philip S. Justus, NMSS/DWM/HLWB
Mail Stop 7 C6
Two White Flint North
11545 Rockville Pike
Rockville, MD 20852-2738

Subject: Transmittal of Strain Distribution and the Tectonic Setting of Yucca Mountain and Crater Flat—Journal Article retitled Composite 13 million year record of extensional faulting and basin growth of Crater Flat Nevada (IM 01402.471.020)

Dear Dr. Justus:

The purpose of this letter is to transmit Intermediate Milestone 01402.471.020 Strain Distribution and the Tectonic Setting of Yucca Mountain and Crater Flat—Journal Article. To more accurately reflect the contents of the paper it has been retitled: Composite 13 million year record of extensional faulting and basin growth of Crater Flat, Nevada. Upon receiving NRC acceptance we plan to submit this manuscript to the Bulletin of the Geological Society of America.

The conceptual model developed in this manuscript defines Yucca Mountain as part of the Crater Flat structural basin. The manuscript demonstrates that the most active period of basin development was between 11 and 12 Ma. Since that time, Crater Flat basin has remained tectonically active at a significantly lower rate. The tectonic model integrates geological and geophysical data including paleomagnetic record of rotations, aeromagnetic and gravity data and geological data of rock-avalanche deposits exposed in wells and in outcrop in southern Crater Flat. More importantly, the manuscript establishes a structural tectonic framework that relates deformation at Yucca Mountain directly to past geologic activity of the Bare Mountain fault. This connection is important because in addition to the Bare Mountain fault being a potential seismic source, the fault may also directly control faulting and fracturing at Yucca Mountain.

This model is an elaboration of the half graben with deep detachment tectonic model that was considered viable in the Issue Status Resolution Report for Structural Deformation and Seismicity, Revision 2 issued in September 1999. That subissue remains closed. The development of this model has been one component in the KTI's plan to resolve outstanding seismic and fault displacement hazard subissues with the DOE. In particular, the tectonic model outlined in this manuscript proposes that many of the faults near Yucca Mountain may not penetrate the entire crust, as was conservatively assumed in the DOE's PSHA study. Moreover, the model provides further proof that the GPS strain rate of Wernicke et al. (1998) is anomalous and not representative of the seismic hazard at Yucca Mountain. Hence,

Washington Office • Twinbrook Metro Plaza #210
12300 Twinbrook Parkway • Rockville, Maryland 20852-1606

this model provides an important technical justification that will allow the SDS KTI to resolve remaining open subissues in seismicity and faulting.

If you have any questions please contact Dr. John Stamatakos at (210) 522-5247 or me at (210) 522-5183.

Sincerely,

H. Lawrence McKague
Element Manager, Geology and Geophysics

HLM/adm
Enclosure

cc:	J. Linehan	W. Reamer	D. Sims
	D. DeMarco	W. Patrick	P. La Femina
	B. Meehan	CNWRA Directors	D. Ferrill
	J. Greeves	CNWRA Element Managers	M. Gray
	J. Holonich	P. Maldonado	C. Hall
	S. Wastler	T. Nagy	A. Morris
	D. Brooks	J. Stamatakos	D. Waiting
	J. Trapp	B. Hill	C. Connor

D:\ANNETTE\Stamatakos\IM\IM471-020\471-020js-Ltr.wpd

Composite 13 million year record of extensional faulting and basin growth of Crater Flat, Nevada

John A. Stamatakos
Brittain E. Hill
David A. Ferrill
Peter La Femina
Darrell Sims
Charles B. Connor

Center for Nuclear Waste Regulatory Analyses, Southwest Research Institute™, San Antonio, Texas 78238

Mary Beth Gray — *Department of Geology, Bucknell University, Lewisburg, Pennsylvania 17837*

Alan P. Morris — *Division of Earth and Physical Sciences, University of Texas at San Antonio, San Antonio, Texas 78249*

Chris M. Hall — *Department of Geological Sciences, University of Michigan, Ann Arbor, Michigan 48109*

ABSTRACT

Crater Flat basin in southwestern Nevada encompasses the site of the nation's proposed high-level radioactive waste repository at Yucca Mountain. The timing and nature of extensional deformation within Crater Flat basin must be considered in evaluation of hazards related to seismicity, faulting, and basaltic volcanism during the 10,000-yr performance period of the proposed repository. Paleomagnetic, radiometric, and geochemical data augment extensive geological and geophysical data for this area, which are used to develop a new tectonic model for the Crater Flat

basin that explicitly incorporates deformation related to outer-arc extension of the hangingwall above a listric fault, including vertical-axis rotations related to extensional deformation. This new model demonstrates that most of the post-15-Ma extension of Crater Flat basin occurred between 12 and 11 Ma. Rapid extension of the Crater Flat basin is demonstrated by the largest differences in degree of vertical axis rotation occurring between units older than about 12 Ma and those younger than about 11 Ma. These vertical axis rotations originate by extensional deformation as the result of southward increases in dip of the listric Bare Mountain fault, which is the hangingwall fault for the western Crater Flat basin. Other evidence for rapid extension includes new geophysical modeling that indicates a thick accumulation of 11.6 ± 0.1 Ma Rainier Mesa Tuff was deposited in a rapidly developed half-graben basin adjacent to the Bare Mountain fault. Rapid extension and basin subsidence enhanced exposure of the Bare Mountain footwall block, resulting in an over-steepened topography. These over steepened Bare Mountain exposures collapsed several times producing rock avalanche megabreccia deposits in Crater Flat basin. Subsequent alluvial sedimentation in Crater Flat basin also represents an unroofing sequence of Bare Mountain consistent with an over-steepened topography and an eastward then westward progradation of the basinal depocenter that reflects a high then low clast production rate at Bare Mountain. Cumulative throw across the Bare Mountain fault between about 12 Ma and 11 Ma ranges from 1 to 2 km, suggesting a fault-slip rate of 1–2 mm/yr. After about 11 Ma, this slip rate likely reduced to present

rates of about 0.06 mm/yr. This composite geologic record of Crater Flat basin provides a fundamental component in the evaluation of the volcanic and seismic hazards at Yucca Mountain.

INTRODUCTION

Geological and geophysical investigations of Crater Flat basin, Nevada, provide one of the most complete records of extensional faulting and associated basin growth within the Basin and Range Province. Compared to highly extended regions to the north and west (e.g., Wernicke et al., 1988), overall extension in Crater Flat basin is modest and appears not to have been affected by a phase of large-scale detachment faulting common in the more highly extended regions of the desert southwest. As such, Crater Flat basin preserves elements of a nascent continental basin.

The details of available data and observations are the result of the extensive characterization of Yucca Mountain for U.S. Department of Energy (DOE) by the United States Geological Survey (USGS) and associated government agencies (e.g., Carr, 1982, 1984, 1990; Snyder and Carr, 1984; Carr and Parrish, 1985; Scott, 1990; Oliver and Fox, 1993; Brocher et al., 1998; Fridrich et al., 1999; Fridrich, 1999). Additional information comes from evaluation of the DOE characterization by the Center for Nuclear Waste Regulatory Analyses on behalf of the Nuclear Regulatory Commission (e.g., Connor et al., 1999, 2000; Ferrill et al., 1996a, 1996b, 1997, 1998, 1999a, 1999b; Stamatakos et al., 1997, 1998; Stamatakos and Ferrill, 1998). Yucca Mountain, as part of the Crater Flat basin (Figure 1), currently is the only

candidate site being considered by the DOE for permanent disposal of high-level radioactive waste (National Research Council, 1995).

The topographic expression of Crater Flat does not bound the structural extent of Crater Flat basin. Previous geological and geophysical studies clearly identify Bare Mountain as the western bound of Crater Flat basin, which is marked by the Bare Mountain fault, a large-displacement normal fault containing a footwall block of Precambrian and Paleozoic sedimentary and metamorphic rocks (Figure 1). In contrast, the eastern boundary of Crater Flat basin is diffuse. Although the Solitario Canyon fault (Figure 1) marks the eastern extent of alluvium within topographic Crater Flat, similar magnitude faults occur to the east (Brocher et al., 1998). Gravity and aeromagnetic data (e.g., McCafferty and Grauch, 1997) show the eastern bound of Crater Flat basin coincides with a marked north-trending anomaly beneath Jackass Flat, informally named the Gravity fault. In this paper we follow the definition of Fridrich (1999) and consider Yucca Mountain to constitute a central graben high that is part of the Crater Flat basin. Although the southern extent of the Crater Flat structural basin is poorly constrained, gravity data (e.g., McCafferty and Grauch, 1997) also show that the basin likely extends at least 30 km south of the low-lying hills that bound the Crater Flat topographic basin (Figure 1). The northern boundary of Crater Flat basin abuts Tertiary volcanic rocks of the Timber Mountain caldera complex (Figure 1).

Extensional faulting in the Crater Flat basin began in the middle Miocene (perhaps earlier), predating eruption of the large-volume silicic pyroclastic deposits and lavas from the Southwest Nevada Volcanic Field (SNVF) (e.g., Christiansen et al., 1977). Evidence for middle Miocene extension includes basinal control of ignimbrite deposition (Byers et al.,

1976a) and emplacement of a series of north-trending 14.9–13.8 Ma porphyry dikes in Bare Mountain (e.g., Weiss, 1996). Over 7,000 km^3 of silicic magma erupted from the SNVF between 15.3 and 11.5 Ma (Sawyer et al., 1994). Extension occurred during the eruptions, with significant unconformities developing between 12.7 and 11.6 Ma (Christiansen et al.,1977; Sawyer et al., 1994). Regionally extensive basaltic magmatism followed the late stages of caldera activity to about 7 Ma (Crowe, 1986). A period of large-scale detachment faulting on the Fluorspar Canyon fault (Figure 1), part of the regional Bullfrog Hills detachment system, occurred during or after the latest stage of silicic volcanism (cf. Sawyer et al., 1994; with Maldonado, 1990). The Fluorspar Canyon-Bullfrog Hills detachment extends the Miocene volcanic rocks along northern Bare Mountain and in the Bullfrog Hills by as much as 275% (Maldonado, 1990). Since late Miocene time, Bare Mountain and the adjoining basins continued to extend and subside at significantly lower rates (Fridrich, 1999). Basaltic volcanism since about 7 Ma occurred mainly within Crater Flat basin and the Amargosa Desert (Figure 1) with important episodes of activity at 3.8 Ma, 1.0 Ma, and 77 ka (Fleck et al., 1996; Champion, 1995; Heizler et al., 1999). Undated episodes of basaltic magmatism are represented by the numerous high-amplitude aeromagnetic and ground magnetic anomalies in the region (e.g., Connor et al., 1997). Distribution of basaltic volcano clusters appears to be structurally controlled by both shallow and deep crustal faults (e.g., Connor et al., 2000).

In addition to extension, the western reaches of the Basin and Range Province contain numerous, mainly northwest-trending, dextral strike-slip faults. Collectively these strike-slip faults and intervening normal faults are referred to as the Walker Lane (Figure 1) (Stewart, 1988; Oldow et al., 1994). Deformation within the Walker Lane is manifested by kilometer-

scale translation of upper crustal blocks coupled with rotations about horizontal, steeply inclined, and vertical axes. Major structural features of this deformation include pull-apart basins such as Death, Saline, and Panamint Valleys.

Vertical-axis rotations of crustal blocks within the Walker Lane have been documented by paleomagnetic results. For example, Cenozoic and Permian-Triassic secondary magnetizations in Paleozoic carbonate rocks and primary magnetization in Cenozoic clastic and volcanic deposits reveal as much as 100° of clockwise rotation associated with motion along the Las Vegas Valley shear zone (Gillett and Van Alstine, 1982; Nelson and Jones, 1987; Sonder et al., 1994). Significant clockwise rotations are also observed in the Black and Cottonwood Mountains (Holm et al., 1993). Within Crater Flat basin vertical-axis rotations are recorded within the Miocene tuffs (Rosenbaum et al., 1991; Hudson, 1992; Hudson et al., 1994; Minor et al., 1997; Fridrich et al., 1999). In contrast, rocks within adjacent basement footwall blocks at Bare Mountain and the Striped Hills have not rotated since at least the late Miocene and possibly since the Permian (Stamatakos et al., 1998).

In this paper we summarize the history of extensional deformation within Crater Flat basin and examine the relationship of extensional and possible transtensional processes to the growth of Crater Flat basin. We develop a record of extensional deformation and basin growth based on the existing published data augmented with new radiometric ages, paleomagnetic results, geochemical analyses, geophysical data, and structural and geophysical interpretations. In particular, we show that Miocene basalt and overlying carbonate megabreccia deposits observed in outcrops of southern Crater Flat basin (herein referred to informally as the Will Carr Hills) and in one of the two USGS deep wells drilled in

Crater Flat are important geological units in deciphering the complex geology of this basin. Much of the new interpretation relates analyses of the timing and mechanisms of vertical-axis rotations recorded by paleomagnetic data to extensional rather than strike-slip deformation. Details of the data, analyses, and interpretations bear on our understanding of extensional tectonics, especially with regard to the beginning of basin subsidence and growth and the evolution of bounding fault systems. Temporal and spatial development of these fault systems also influences estimates of future seismic and volcanic hazards for the potential Yucca Mountain repository. In particular, insights gained from these new tectonic interpretations helps us better constrain uncertainties in current DOE estimates of the seismic and volcanic hazard at Yucca Mountain (U.S. Geological Survey, 1998; Geomatrix, 1996).

GEOLOGIC FRAMEWORK

Rocks and sediments of the Crater Flat region, including Bare Mountain and the Crater Flat basin, span geologic time from the Late Proterozoic to the present (Figure 2). The ensuing summary groups rocks and sediments of the Crater Flat region into five informal stratigraphic successions that reflect this paper's emphasis on the Miocene deformational history of Crater Flat: (1) basement rocks consisting of Precambrian and Paleozoic clastic and carbonate rocks with minor occurrences of Mesozoic and Tertiary igneous and meta-igneous sills, dikes, and flows; (2) Miocene silicic volcanic rocks; (3) Miocene basaltic volcanic rocks; (4) Miocene megabreccia deposits; and (5) late Tertiary and Quaternary fluvial, alluvial, colluvial, and landslide deposits interbedded with Pliocene to Late Quaternary

basalt. Although Oligocene(?) to Early Miocene rocks occur in some drill holes deeper than about 1,500 m, they are not observed in outcrop in Crater Flat basin and thus are not included in this summary.

Basement Rocks

Precambrian and Paleozoic sedimentary and meta-sedimentary rocks exposed on Bare Mountain are multiply deformed. In addition to the two or more phases of Late Miocene-to-present extensional deformation, basement rocks experienced contraction deformation in the Permian (Snow, 1992), Mesozoic (e.g., Armstrong, 1968). Earlier extensional deformation predates eruption of the SNVF (e.g., Ekren et al., 1971; Christiansen et al., 1977) and is possibly related to Eocene extension of the Basin and Range (Axen et al., 1993). Later deformation is associated with Late Miocene Basin and Range extension (Wernicke et al., 1988). The resulting structure of basement rocks at Bare Mountain (e.g., Monsen et al., 1992) is a complex of steeply dipping folded and faulted rocks. The structure of pre-Miocene basement rocks beneath the Crater Flat basin is not known. Because deformation at Bare Mountain predates dip-slip motion on the Bare Mountain fault (Ferrill et al., 1998; Stamatakos et al., 1998; Fridrich, 1999), basement rocks beneath Crater Flat basin are presumably folded, faulted, and eroded, analogous to the deformation expressed at Bare Mountain.

Miocene Silicic Volcanic Rocks

Miocene volcanic rocks, mainly silicic tuffs, are up to 5 km thick and except on Bare Mountain obscure most of the basement rocks in the intra-basinal areas. Most of the SNVF silicic volcanism occurred between 15.2 and 11.4 Ma and peaked between 12.8 and 11.4 Ma (Christiansen et al., 1977; Sawyer et al., 1994). Thickness variations for these tuffs provides additional insights into the development of Crater Flat basin. Tuffs of the Crater Flat Group show changes in thickness over relatively short distances. Some sections of 13.3 ± 0.02 Ma Bullfrog Tuff proximal to the eruptive source, for example, are significantly thinner than incompletely preserved sections located 10 to 20 km distally from the source, indicating a depositional basin was well established in western Crater Flat basin by this time (e.g., Byers et al., 1976a; Christiansen et al., 1977). In contrast, the overlying Topopah Spring Tuff shows a relatively consistent proximal-to-distal thinning, suggesting little basinal subsidence following infilling by the Crater Flat Group tuffs. The Yucca Mountain area likely represents a paleotopographic highland during deposition of the Pah Canyon and Yucca Mountain tuffs (Lipman and Christiansen, 1964), which are well preserved in a sector northwest to southwest of Yucca Mountain.

Carr (1982) reported silicic pumice with a zircon fission-track date of 6.3 ± 0.8 Ma in poorly indurated alluvium beneath Pliocene basaltic lavas in Crater Flat. He speculated that this pumice may correlate with an undiscovered silicic volcanic center in Crater Flat. The pumice deposit consists of subangular to subrounded lapilli with an average maximum diameter of 4.4 cm, although several 6-cm-diameter blocks occur. At least two 10 to 15 cm-

thick interbeds of matrix-free reworked pumice occur within a massive, medium-to-coarse grained sandy paleosol sequence that is extensively bioturbated. Feldspar separates from larger pumice lapilli yield a single-crystal $^{40}Ar/^{39}Ar$ date of 9.0 ± 0.3 Ma at two sigma uncertainty (Appendix 1). This date correlates with several large-volume pyroclastic eruptions from the Black Mountain caldera between 9.2 and 9.4 Ma (Sawyer et al., 1994). Pumice blocks (i.e., ≥6 cm) in tephra falls are generally restricted to less than 40 to 50 km from the source vent (e.g., Carey and Sparks, 1986), which is consistent with eruption 30 to 40 km to the northwest from the Black Mountains. Therefore, the Crater Flat pumice most likely represents a locally reworked tephra-fall deposit of the Thirsty Canyon Group from the Black Mountain caldera.

Miocene Basalt

Miocene basaltic lavas, dikes, and scoria overlie and intrude 11.45 Ma Ammonia Tanks Tuff in the Will Carr Hills (Swadley and Carr, 1987). The basalt in the Will Carr Hills was originally dated at 10.5 ± 0.1 Ma using K/Ar (R.J. Fleck written communication to Swadley and Carr, 1987). Recent ground magnetic surveys (Connor et al., 1997), however, indicated the lavas in the Will Carr Hills have a reversed-polarity magnetization. A reversed-polarity magnetization is inconsistent with a 10.5 ± 0.1 Ma K/Ar date because the geomagnetic polarity time scale (GPTS) of Cande and Kent (1992) shows normal polarity of the Earth's geomagnetic field in the interval between 9.78 and 10.83 Ma (chron C5n.2n). We obtained new dates of the exposed basalt based on $^{39}Ar/^{40}Ar$ isotopic analysis of 11.2 ± 0.4 Ma

(Appendix 2), which represents an age consistent with the reversed polarity geomagnetic field during chrons C5n.2n or C5r.1r.

A 30-m thick section of basalt, dated by K/Ar at 11.3±0.4 Ma, also directly overlies the 11.45 ± 0.03 Ma Ammonia Tanks Tuff in drill hole USW VH-2 (Carr and Parrish, 1985). The USW VH-2 basalt has a strongly reversed-polarity magnetization (Carr and Parrish, 1985) and is compositionally similar to basalt in the Will Carr Hills (Appendix 3). We agree with previous workers (e.g., Carr and Parrish, 1985; Crowe, 1986) that USW VH-2 basalt correlates directly with basalt in the Will Carr Hills. We therefore estimate an age for the basalt at both locals of 11.1 ± 0.3 Ma, which best represents the most reliable geochronologic, stratigraphic, geochronological, and paleomagnetic data.

Miocene basalt dikes also are exposed along the Solitario Canyon fault near Yucca Mountain within 12.7 ± 0.3 Ma Tiva Canyon Tuff (Day et al., 1997, 1998). These basaltic dikes are compositionally distinct from other Miocene basalt in Crater Flat basin (Appendix 3). Reported radiometric dates for these dikes are 11.7 ± 0.3 Ma (Smith et al., 1997) and 10.0 ± 0.4 Ma (Crowe et al., 1983). The magnetic anomaly associated with the Solitario Canyon dikes indicates a normal polarity (Magsino et al., 1998), consistent with normal-polarity chrons of 9.78–10.83, 10.94–10.99, or 11.38–11.43 Ma, based on the geomagnetic time scale of Cande and Kent (1992).

Miocene Megabreccia Deposits

In the Will Carr Hills, Miocene basaltic flows and dikes are capped by at least 85 m (and possibly as much as 200 m according to Swadley and Carr, 1987) of megabreccia (Figures 1 and 3). The megabreccias, interpreted as subareal landslides or rock avalanche deposits, are composed of Cambrian Bonanza King and Carrara limestones with minor blocks of dolomite and schist (Swadley and Carr, 1987). The exposed megabreccias are extensive and cover a large portion of the Will Carr Hills (Figures 1 and 3A–3C). These landslide deposits probably include Black Marble, a single gravity-slide block of Cambrian carbonate rock adjacent to the southern tip of Bare Mountain (Swadley and Carr, 1987). Monsen et al. (1992) map Black Marble Mountain as the hangingwall of a detachment that places it on top of the lowest member of the Precambrian Stirling Quartzite, the oldest rocks exposed at Bare Mountain. Unlike the megabreccia deposits in the Will Carr Hills, stratigraphy in Black Marble Mountain remained coherent, but disturbed, cut by numerous fractures, small faults, and veins, and tightly folded by meso and micro-scale fold that may be related to its detachment.

Similar megabreccia deposits were encountered in USW VH-2, including two or three between the 12.7 ± 0.03 Ma Tiva Canyon and 11.6 ± 0.03 Ma Rainier Mesa tuffs and one directly above a thick section of 11.1 ± 0.3 Ma basalt overlying the Ammonia Tanks Tuff (Figure 4A). Analogous to the exposures in southern Crater Flat, the uppermost megabreccia (what we refer to as MB1 in Figure 4A) in USW VH-2 appears monolithologic, composed of Cambrian carbonate rocks of the Bonanza King Formation (cf. Figures 3D with 4C). Given

these relationships, we conclude that the basalt-MB1 megabreccia sequence in USW VH-2 and the one exposed in the Will Carr Hills are correlative and that much of the western Crater Flat topographic alluvial basin is underlain by these two lithologies (Figure 1). In outcrop, the contact between the megabreccia and underlying basalt is sharp, without evidence of visible soil development or sediment accumulation between deposition of the basalt and emplacement of the magebreccia. In USW VH-2, however, the contact contains a 6-cm-thick horizon of polylithologic pebbly silts and sands (Figure 4D) with internal shear bands that likely represents a thin sequence of alluvial deposit subsequently deformed by the emplacement of the overlying megabreccia.

The older megabreccias in USW VH-2 which we refer to as MB2, MB3, and MB4 in order of their appearance down hole (Figure 4A) are also composed of carbonate rock clasts. Similar to MB1, MB2 is composed of rock clasts appearing to have been derived from the Bonanza King Formation. MB2 lies directly beneath the Rainier Mesa Tuff with a sharp contact (Carr and Parrish, 1985) and, thus, we suggest it was emplaced immediately before 11.6 Ma. MB3 and MB4 are contiguous with each other and separated from the bottom of MB2 and from the top of the Tiva Canyon Tuff by sections of alluvium. Hence, the exact age of the emplacement of MB3 and MB4 is less certain. Carr and Parrish (1985) also note that MB3 and MB4 contain carbonate clasts derived from the Ordovician Antelope Valley Formation. Thus, MB3 and MB4 were probably derived from northern Bare Mountain, where Antelope Valley Formation rocks are exposed (Monsen et al., 1992).

The areal extent of the upper megabreccia (including MB1) may be as large as 125 km^2, based on the area of Crater Flat bound by the Bare Mountain fault, Will Carr Hills,

drill hole USW VH-2, and the northern limit of carbonate rock exposure at Bare Mountain (Figure 1). Given constraints on megabreccia [i.e., thickness, 200+ m based from mapped outcrop thickness and description given in Swadley and Carr (1987) and 51 m in USW VH-2 (Carr and Parrish, 1985)], the corresponding volume of megabreccia buried in Crater Flat is impressive. If we assume a simple tapered wedge and 30% inflation from porosity gain in the megabreccia, we estimate an initial volume between 5 and 15 km^3. Black Marble Mountain, if considered part of this megabreccia, adds an additional 0.1 km^3. Given the present outcrop pattern of Bare Mountain (Monsen et al., 1992), this volume of megabreccia would require 300–900 m of additional elevation of the Bonanza King Formation at Bare Mountain above its present exposure.

Late Tertiary and Quaternary Deposits and Pliocene to Late Quaternary Basalt

Pliocene and Quaternary deposits in Crater Flat basin consist mainly of unconsolidated alluvium, colluvium, debris-flow, and eolian deposits. The stratigraphy of these units in Crater Flat and adjacent to Bare Mountain have been developed by Swadley and Parrish (1988), Faulds et al. (1994), and Peterson et al. (1995). Corresponding maps of the surface distribution of these units generally show progressively younger deposits toward the southern end of Crater Flat basin, consistent with interpretation that the southern part of the basin subsided at a faster rate than other portions of the basin since at least about 1.0 Ma (Stamatakos et al., 1997). Neogene and Quaternary deposits are intruded by and interbedded with a series of Pliocene and late Quaternary basaltic dikes and volcanoes.

Pliocene volcanism, dated at 3.7 ± 0.2 Ma (Fleck et al., 1996), was primarily confined to the eastern portion of Crater Flat basin. Quaternary volcanism include an alignment of at least four coeval volcanic cones in western Crater Flat, dated at about 1.0 ± 0.2 Ma (Fleck et al., 1996) and the Lathrop Wells basaltic cone dated by K/Ar at 77 ± 5 ka (Heizler et al., 1999). In addition, numerous aeromagnetic anomalies have been identified in Crater Flat basin and the Amargosa Desert as buried basalt (Figure 1) (Langenheim, 1995; Connor et al, 1997, 2000).

Alluvial deposits in both USW VH-1 and USW VH-2 also show significant changes in composition that probably reflect tectonically induced changes in the clast source (Figure 4). In USW VH-2, carbonate rocks dominate the alluvium from 309 to 283 m. Clast composition changes to quartzites and siltstones from a 283- to 131-m depth and back to carbonate rocks with minor volcanic clasts from a 131- to 107-m depth. Miocene tuffaceous volcanic rocks dominate the alluvium from a 107-m depth to the surface. The alluvial matrix, however, is dominantly volcanic in origin above a 283-m depth. A similar carbonate rock to tuff-derived transition is observed in USW VH-2 at approximately a 90-m depth.

We interpret these changes to reflect unroofing of Bare Mountain by erosion as the source rocks changed from carbonate rocks to quartzites and siltstones and back to carbonate rocks. The Crater Flat basin depocenter prograded eastward to the location of USW VH-1 by the time the carbonate rocks were being incorporated into the alluvium a second time. We suggest the sedimentation rate exceeded the rate of basin subsidence during this interval. Erosion of nonwelded to poorly welded tuffs that mantled the surrounding area provided the fine-grained matrix for the alluvial deposits.

With continued basin subsidence, but lower rate of clast production from Bare Mountain, the basinal depocenter regraded westward. Downward incision in response to basin subsidence eroded more densely welded tuffs, producing the tuffaceous clasts. By the Late Pliocene, the alluvium is dominantly volcanic, with the main depocenter still located in western Crater Flat as shown by the dominantly fine-grained sediments beneath 3.8 Ma lavas in eastern Crater Flat and the significantly coarser sediments beneath correlative lavas in USW VH-1.

Structure

Tuffs of the Crater Flat basin generally are flat-lying or moderately tilted in fault blocks bound by normal faults, except along the northern margin of Bare Mountain. There, detachment faulting on the Fluorspar Canyon fault (Figure 1), as part of the Bullfrog Hills detachment system, appreciably attenuates the Miocene section. Overall deformation of these tuffs at Yucca Mountain is expressed as a sequence of north- to northeast-trending, fault-bound ridges crossed by occasional northwest-trending, dextral strike-slip faults (Figure 1). Faults dip almost uniformly to the west and separate blocks of gentle to moderate east-dipping tuff. From north to south, both fault displacement and stratal tilt increase and indicate progressively greater extension of the Crater Flat basin southward (e.g., Scott, 1990). This pattern is best expressed on the west flank of Yucca Mountain, which is defined by a series of left-stepping and north-trending *en echelon* faults (Day et al., 1998; Ferrill et al., 1999a).

Linkage of the *en echelon* system is either by lateral propagation of curved fault tips or formation of connecting faults that breach the relay ramp (Ferrill et al., 1999a; Peacock and Sanderson, 1994; Trudgill and Cartwright, 1994). The *en echelon* pattern of faulting is best expressed along the western edge of Yucca Crest and the fault line escarpment that follows the west-dipping Solitario Canyon, Iron Ridge, and Stagecoach Road faults (Simonds et al., 1995). The geometry of these faults and ridges defines a scallop trend, composed of linear, north-trending fault segments connected by discrete curvilinear northwest-trending fault segments. For example, the end of the northwest-trending curvilinear Iron Ridge fault bends to the northwest near its overlap with both the Stagecoach Road and Solitario Canyon faults (Figure 1). Yucca Mountain also contains numerous swarms of small northwest-trending faults that connect the large north-trending faults. One example is at West Ridge, which is cut by numerous northwest-trending small faults that connect segments of the north-trending Windy Wash and Fatigue Wash faults. This fault geometry strongly suggests that the entire Yucca Mountain fault system is an *en echelon* branching fault system (Ferrill et al., 1999a) in which faulting on the large block-bounding fault triggers relatively widespread, but predictable, secondary faulting on connecting and linking faults.

GEOPHYSICAL FRAMEWORK

Extensive geophysical investigations have been completed across the Crater Flat region, including reflection seismic (Brocher et al., 1998) and several generations of gravity, aeromagnetic, and ground magnetic studies (e.g., Snyder and Carr, 1984; Oliver et al., 1995;

Langenheim and Ponce, 1995; Blakely et al., 1999; Stamatakos et al., 1997; Connor et al., 1997, 2000). Of these survey methods, gravity and magnetics prove the most useful in imaging details of the subsurface structures and stratigraphic relationships. Gravity anomalies point to density contrasts between basement rocks and the less dense tuff and alluvium that fill the basins. Magnetic anomalies point to contrasts in the strong remanent magnetizations of the Miocene Tuffs and the younger basalt with essentially nonmagnetic basement rocks and valley-fill sedimentary deposits. In contrast, interpretations of the reflection seismic surveys are equivocal, confounded by strong reflections in the highly folded and faulted bedding of the Precambrian and Paleozoic basement bedding beneath Crater Flat.

Gravity

Gravity data confirm the importance of the Bare Mountain fault as a regional structure, indicated by the 36 mGal complete Bouguer gravity anomaly across the fault (Figure 5A). This gravity anomaly continues south into the Amargosa Desert, perhaps an extension of the basin south of the topographic limit of the Crater Flat basin. Gravity anomalies are less distinct on the east side of Crater Flat. An approximate 10-mGal anomaly extends north of Lathrop Wells volcano, roughly parallel to the Stagecoach Road fault and then north through Yucca Mountain, parallel to the Solitario Canyon fault (Figure 5A). Further southeast, the Gravity fault is a 15-mGal, north-trending anomaly that continues into Fortymile Wash. Together, gravity anomalies associated with the Bare Mountain fault and those on the eastern side of the Crater

Flat basin and the Amargosa Desert form a north-south-trending gravity depression, often termed the Amargosa Gravity Trough (O'Leary, 1996). This trough extends northward to intersect a dramatic gravity low at the Timber Mountain caldera (Snyder and Carr, 1984). Basaltic volcanism during the Pliocene through Quaternary has been limited to this trough, suggesting this large crustal feature may influence or reflect the generation or segregation of small-volume, lithospheric, basaltic magmas (Connor et al., 2000).

Inversion of gravity anomalies by Langenheim and Ponce (1995), Blakely et al. (1999), and Brocher et al. (1998) suggest an accumulation of 5–6 km of Cenozoic rocks in southern Crater Flat (Snyder and Carr,1984). In detail, gravity anomalies suggest an increase in dip of the Bare Mountain fault, from north to south. The average horizontal gravity gradient in the northern part of Crater Flat is on the order of 3 mGal/km. That gradient more than doubles to 6–8 mGal/km in the southern part of the basin, west and south of Red Cone and Black Marble Mountain. Simple forward models suggest this change in gravity gradient corresponds to a change in fault dip from approximately 45° in the northern part of the basin to greater than 70° in the south. This change in fault dip also correlates well with the estimated change in basin depth (Langenheim and Ponce, 1995; Blakely et al., 1998).

Magnetic

Aeromagnetic anomalies (Figure 5B) reveal marked contrast in the magnetic properties of rocks across the Bare Mountain fault (Kane and Bracken, 1983). Similar to the gravity data, the horizontal magnetic gradient is greatest in the southern part of the basin,

implying a thicker accumulation of comparatively highly magnetized tuff than in the northern part of the basin. A broad positive magnetic anomaly dominates the southern third of Crater Flat (Kane and Bracken, 1983). This anomaly was originally interpreted as evidence for a caldera in Crater Flat (Snyder and Carr, 1984). More recent age dates for the entire sequence of the SNVF (Sawyer et al., 1994) indicate that all caldera centers, including those for the Crater Flat tuffs, have been identified north of Crater Flat.

Most recently, this positive anomaly has been modeled as 11.1 ± 0.3 Ma basalt overlying the weakly magnetized Paleozoic section at less than a 3-km depth, or as highly magnetic and displaced Mississippian-Devonian Eleana Formation (Brocher et al., 1998). These interpretations, however, are not supported completely by the existing data. The 11.1 ± 0.3 Ma basalt cited as the source for the negative anomaly has a reversed polarity magnetization and is present in USW VH-2, which lies within the positive anomaly of southern Crater Flat (Figure 5B). Magnetic Eleana is found in drill holes in the Calico Hills north of Yucca Mountain, however, no mineralized Eleana is observed on Bare Mountain. Moreover, the distribution of Bedrock at Bare Mountain (Monsen et al., 1992) indicates that Pre-Cambrian and Cambrian rocks and not the Mississippian-Devonian Eleana Formation underlie most of Crater Flat basin.

Paleomagnetism

Extensive paleomagnetic investigations were performed at Bare Mountain (Stamatakos et al., 1998) and in Crater Flat basin (e.g., Rosenbaum et al., 1991; Champion,

1995; Hudson et al., 1994; Fridrich et al., 1999), mainly to determine vertical- or inclined-axis rotations related to Miocene to present deformation. Vertical-axis rotations from these studies are summarized in Figure 6. In the Miocene tuff section, we excluded results from the Topapah Springs Tuff because site mean directions from those rocks show large dispersions, especially in inclination. Rosenbaum (1986) suggested that subblocking temperature compaction corrupted the reliability of the remanence vectors in these rocks, although inadequate averaging of secular variation of the geomagnetic field can not be ruled out. The existing published data are augmented by new results from the Miocene basalt and megabreccias in the Will Carr Hills (Appendix 4) and Pliocene flows of Crater Flat (Connor et al., unpublished data).

The data show that vertical or inclined-axis rotations are most prevalent in Tiva and older tuff units exposed in southern Yucca Mountain and along the Will Carr Hills. Data from Bare Mountain do not show significant rotations, including a secondary Permian-Triassic magnetization in the Ordovician carbonate rocks (Stamatakos et al., 1998). With few exceptions, most of the site mean directions are not significantly rotated in northern Crater Flat or northern Yucca Mountain. Magnetic directions from the Pliocene flows of Crater Flat appear to show a slight counter-clockwise rotation, but this may reflect incomplete averaging of secular variation rather than a tectonic origin (Champion, 1995). The one exception is from a site within a detached block lying on the footwall of the south Crater Flat fault that records a 93° clockwise rotation. This site was drilled in the exposed footwall of one of the USGS paleoseismic trenches across the south Crater Flat fault. We interpret this site as a loose block of basalt, which we initially mistook for intact bedrock.

Within the Will Carr Hills, the rocks show an interesting progression of rotations that appear to record the onset and end of rotation. In the Will Carr Hills, two site-mean directions from the 12.7 ± 0.03 Ma Tiva Canyon Tuff indicate up to 34° of clockwise rotation (Fridrich et al., 1999; Hudson et al., 1996). The younger 11.6 ± 0.03 Ma Rainier Mesa Tuff shows approximately 35° of clockwise rotation, but the 11.45 ± 0.03 Ma Ammonia Tanks Tuffs show significantly smaller rotations of approximately 20°. The 11.1 ± 0.3 Ma basalt shows an average clockwise rotation of 12°, while the remagnetized megabreccia are essentially unrotated. These data suggest that the clockwise rotations of these rocks occurred rapidly (Figure 7), within approximately a 600-kyr period between 11.6 and 11.0 Ma, yielding a rotation rate of 5.8° per 100,000 kyr.

Rotations of remanent magnetization directions about a vertical axis are most commonly associated with block rotations along strike-slip faults (e.g., Stamatakos, 1988). Rotations of crustal blocks about vertical or inclined axes also were interpreted in thrust fault systems (e.g., Van der Voo et al., 1997). We previously showed that for Crater Flat, the pattern of rotations documented by the Miocene tuffs is best explained by vertical or inclined axes rotations associated with extensional faulting (Stamatakos and Ferrill, 1998). Our model suggests that hangingwall segments, especially relay ramps on normal or oblique faults with large throw gradients, cause the hangingwall to rotate. In particular, normal fault systems with fault traces that are segmented and *en echelon* often show displacements that vary significantly along traces of individual fault segments (Willemse, 1997). Fault displacements grade from zero at the fault tips of a single fault to some maximum between the tips. The differential horizontal separation (heave) along a fault trace results in the vertical axis rotation

of the hangingwall or footwall, particularly between the overlapping segments of *en echelon* fault systems (Ferrill et al, 1999a; Ferrill and Morris, unpublished data).

For example, consider the stylized three-dimensional models of normal dip-slip faults shown in Figure 8. Slip on the *en echelon* faults produces hangingwall blocks that dips back into the faults and clockwise rotations about a vertical or inclined axis. Restorations of the hangingwall blocks (and by inference any paleomagnetic site mean directions) to paleohorizontal by a rotation of the dip angles about the lines of strike do not restore the apparent clockwise vertical axis rotations.

In Crater Flat, two areas clearly document these relationships. The first is the faulted relay ramp in the left step between the Solitario Canyon and Iron Ridge faults, called the Iron Ridge Relay (Figure 9A). This system consists of a rotated and tilted relay ramp that has been cut by numerous northwest-trending and southwest-dipping normal faults. Paleomagnetic declinations, fault orientations, and the trend of stratal contacts in the eroded fault gaps all indicate the same pattern—progressive clockwise rotation of fault blocks as a function of total fault slip compared to the unrotated footwall. In southern Yucca Mountain, along the southern segment of the Solitario Canyon fault, the fault system forms a right-stepping relay, with a northward increasing throw gradients. On fault segments here, the largest amount of vertical axis rotation is preserved within a relay ramp, again adjacent to the fault segment with the larger dip-slip displacement gradient (Figure 9B).

NEW INTERPRETATIONS

Structure of Crater Flat Basin Assuming Outer-Arc Extension

The Crater Flat basin is a half graben bounded and generated by the moderately to steeply east-dipping Bare Mountain fault. The basin deepens westward toward the Bare Mountain fault, and its eastern flank is cut by a series of predominantly west-dipping, normal faults exposed within and along the western flank of Yucca Mountain. These west-dipping faults step the Miocene volcanic strata down into the basin. We interpret the half-graben architecture to be the product of slip on the Bare Mountain fault, which we model as a listric normal fault that cuts the brittle crust at relatively high angles and soles into a detachment near the brittle-ductile transition (Figure 10; Ferrill et al., 1996a). Within this structural system, there are several important north to south structural transitions. Surface measurements and geophysical constraints on the dip of the Bare Mountain fault indicate that the fault steepens from 45 to50° at its northern end to ~70° at its southern end. In addition, the pattern of alluvial fan sedimentation indicates progressively younger and more aggradation of alluvial fans along the Bare Mountain front from north to south. The change in alluvial fan morphology is the result of differential throw across the Bare Mountain fault, which is at least partially a function of fault dip (Ferrill et al., 1996b, 1997; Stamatakos et al., 1997).

Along the east flank of the basin, both fault displacement and stratal tilt increase from north to south indicating progressively greater extension of the Crater Flat basin southward (e.g., Scott, 1990; Stamatakos and Ferrill, 1998). This pattern is best expressed on the west

flank of Yucca Mountain, which is defined by a series of left-stepping, north-trending *en echelon* faults (Day et al., 1998; Ferrill et al., 1999a). Vertical-axis rotation of paleomagnetic directions also increases to the south and west (Scott, 1990; Rosenbaum et al., 1991; Hudson et al., 1994).

The hangingwall of a listric normal fault must deform to maintain contact between the hangingwall and footwall fault surfaces and to accommodate the differential hangingwall subsidence produced by displacement along the nonplanar fault. Several geometric-kinematic models can generate compatible fault and deformed hangingwall geometries for listric normal fault systems. These models generally incorporate an assumption of area constant deformation in vertical two-dimensional profiles parallel to the displacement direction. The models are distinguished by their assumptions regarding deformation kinematics for hangingwall deformation. The primary kinematic models are defined by heterogenous simple shear along vertical or steeply inclined directions within the hangingwall (Verrall, 1981; Groshong, 1989; Rowan and Kligfield, 1989; Dula, 1990; Xiao and Suppe, 1992).

Nevertheless, vertical or inclined shear models are limiting because they (1) require layer thinning and extension in deformed parts of the hangingwall; (2) imply that faults cut through the entire hangingwall (surface to detachment); (3) and cannot explain common observed crestal collapse grabens and downward-dipping faults in the hangingwall. Although layer extension is common in normal fault hangingwall, evidence of differential layer thinning related to listric fault hangingwall deformation is not well documented. These limitations occur because layer-parallel shear models were originally developed to model contractional fault-

bend folding (Suppe, 1983) and to incorporate assumptions of preservation of bed length and thickness and no general shear (no net distortion in unbent layers). As noted by Suppe (1983), the application of the technique to normal faulting is restricted to faults with dips or fault bends of 30° or less. Most listric normal faults have ramp angles or fault bends of greater than 30°.

In a revised method (Ferrill and Morris, 1997; Morris and Ferrill, 1999), the constant bed length or no general shear constraint is relaxed to allow for layer extension by normal faulting or extension fracturing in the normal fault hangingwall. The magnitude and distribution of hangingwall deformation above listric normal faults is controlled by displacement, and fault shape. By relaxing the no general shear constraint, deformation of the hangingwall can be modeled as a shear profile (Ferrill and Morris, 1997).

In normal faulting regimes, layer parallel shear of horizontal layers is unlikely because of the large resolved normal stress controlled by a vertical maximum principal compressive stress (typical in normal faulting regimes). In minimum-deformation models, the magnitude of the expected layer length changes in the hangingwall, represented by deflection of the shear profile, and tends to decrease downward from a maximum along the outer arc (uppermost layer) to zero near the base of the hangingwall. This pattern of outer-arc extension explains the common occurrence of crestal collapse grabens and downward-tipping normal faults in the hangingwalls of listric normal faults.

Considering the structure of Crater Flat in the context of outer arc extension in the hangingwall of the southward-steepening Bare Mountain fault provides a consistent explanation for the patterns of displacement and alluvial fan sedimentation along the Bare

Mountain fault, fault displacement and extension in Yucca Mountain (Scott, 1990; Ferrill et al., 1999a), and vertical-axis rotations constrained by paleomagnetic data (Figures 6 and 9). Figure 11 provides a conceptual illustration of the hangingwall deformation (layer-parallel shear or outer-arc extension) for a uniform heave (horizontal extension) on a listric fault that steepens from north to south. A shear profile (Figure 11A) illustrates the net rotation of the back edge of the deformed hangingwall around a vertical axis. In nature this deformation is likely accomplished by outer-arc extension, distributing the vertical-axis rotation across the hangingwall. In the case of Crater Flat, outer-arc extension is accommodated by numerous west-dipping normal faults. Because the dip of the Bare Mountain fault increases from north to south, more outer-arc extension has to be accommodated toward the south end of Crater Flat basin. Thus, faults in the hangingwall of the Bare Mountain fault (those exposed within and along the west flank of Yucca Mountain) that accomplish this extension have increasing displacements to the south (Figure 11B). In addition, each of these northward-tipping normal fault generates a clockwise rotation in its hangingwall as a result of the north to south displacement gradient. The cumulative effect is for net vertical-axis rotations to increase southward and westward (Figure 6) (Stamatakos and Ferrill, 1998).

This mechanical link between the vertical-axis rotations and the deformation of the hangingwall also provides a bound on the age and timing of deformation. The clockwise vertical-axis rotations recorded in volcanic rocks occurred primarily between 11.6 and 11 Ma (Figure 7), thus, a significant pulse of slip on the Bare Mountain fault and the formation of Crater Flat basin must also have occurred during this interval.

Geophysical Modeling

Given new data on the timing of deformation on the Bare Mountain fault, we re-interpreted the potential field data using variations in the thicknesses of tuffs in southern Crater Flat. In particular, we adopt the interpretation of Carr (1982) who proposed that the broad positive magnetic anomaly in Crater Flat (Figure 5B) is produced by differences in the depth, thickness, and magnetization of Bullfrog Tuff. Our interpretation differs from previous ones in that we deduce that the large magnetic low in the basin adjacent to the Bare Mountain fault results from a thick and magnetically intense wedge of normal-polarity Rainier Mesa Tuff.

To test the validity of this interpretation, the expected gravity and magnetic anomalies were calculated along roughly east-west profiles across the Bare Mountain fault (Figures 5A and 5B). Additional constraints were derived from geologic mapping (Day et al., 1997, 1998). The critical elements to our interpretation are (1) the thick Bullfrog Tuff in the center of the basin, (2) the rollover of the Crater Flat basin (hangingwall) into the Bare Mountain fault, and (3) the thick wedge of Rainier Mesa Tuff in the tectonic basin adjacent to the Bare Mountain fault.

Based on this conceptual interpretation, both magnetic and gravity models were constructed (Figure 12). Because of limited gravity data we did not compute models in exactly the same position. In the gravity model, we assumed an average density of 2.5 g/cm^3 for the tuff, alluvium, and basalt in the basin and an average density of 2.75 g/cm^3 for the Paleozoic and Precambrian bedrock of Bare Mountain and the basement below Crater Flat. Results for the gravity model (Figure 12A) show the overall shape of the basin, with the

deepest part of the basin adjacent to Bare Mountain, fits the observed gravity profile. As with previous interpretations (e.g., Snyder and Carr, 1984), our model includes a wedge of bedrock within the Bare Mountain fault zone to account for location of the steepest part of the gravity gradient. The steepest part of the gravity gradient is displaced basinward (east) from the surface trace of the Bare Mountain fault by about 1 km.

The magnetic model is more complicated than the gravity model (Figure 12B) to account for the large variations in the natural remanent magnetizations (both intensity and polarity) of the tuffs. The modeling shows the large positive-negative anomaly in Crater Flat (Figure 6B) can be adequately modeled by variations of the thickness and magnetic properties of the Miocene tuffs. In particular, we ascribe the large positive anomaly to a thick sequence of Bullfrog Tuff accumulated in the central axis of Crater Flat, possibly filling a preexisting topographic low created by pre- or early SNVF faulting or simply preexisting erosional depressions. We interpret the large negative anomaly as a thick accumulation of Rainier Mesa Tuff enhanced by the later deposition of 11.1 ± 0.3 Ma basalt. Both Rainier Mesa Tuff and 11.1 ± 0.3 Ma basalt have strong reversed-polarity remanent magnetizations. We suggest that the thick Rainier Mesa Tuff accumulated in a structural depression created by the rapid pulse of faulting along the Bare Mountain front just prior to emplacement of this tuff unit.

TECTONIC MODEL

The tectonic model we propose follows some of the general trends developed in Fridrich (1999) with regard to overall extension of Crater Flat Basin. The principal differences between the Fridrich (1999) version and the model proposed herein lies in interpretations of the details of the timing of deformation, the mechanism of hangingwall deformation, the listric versus planar style of faulting, the source of the magnetic anomalies in Crater Flat, and the explicit link we develop between extension and vertical-axis rotations, as recorded by paleomagnetic vectors.

Paleomagnetic data and structural models indicate most of the post-15-Ma extension of Crater Flat basin occurred during a geologically brief interval between 12 and 11 Ma. Rapid extension of the basin is supported by several lines of evidence. First, rotation of the paleomagnetic directions reflects deformation of the hangingwall above the Bare Mountain fault. The pattern of hangingwall deformation arose from geometric conditions of the Bare Mountain fault in which horizontal extension of the Crater Flat basin was accomplished by southward increase in fault slip because of southward steepening of the Bare Mountain fault. Steeper portions of the fault require greater fault slip to accomplish the same net horizontal extension. Thus, the timing of the rotations (Figure 7) constrains timing of the hangingwall deformation. Considering uncertainties in the radiometric dates of the tuffs, age of the remagnetization of the megabreccia, and amounts of vertical axis rotations, we propose that the rapid pulse of deformation occurred roughly between 12 and 11 Ma.

Second, geophysical modeling of the pattern of aeromagnetic anomalies in Crater Flat is best explained by a thick accumulation of Bullfrog Tuff in the central part of the basin and a wedge of Rainier Mesa Tuff deposited adjacent to the Bare Mountain fault. We have little geologic evidence to explain why the Bullfrog Tuff is so thick, but we speculate that it accumulated in a trough or basin developed by extensional faulting prior to or synchronous with the earliest stages of the SNVF. The thick accumulation of Rainier Mesa Tuff was deposited in a structural trough developed in a short period by rapid slip on the Bare Mountain fault between 12 and 11 Ma.

Third, rapid deformation exposed a large Bare Mountain footwall block that quickly developed an overly steep and unstable topographic edifice. That edifice subsequently collapsed, at least three times, producing the large volumes of rock-avalanche megabreccia observed in Crater Flat and the Will Carr Hills. Collapses occurred during the development of the structural trough, the first collapse sometime after deposition of the 12.7 ± 0.03 Tiva Canyon Tuff , the second collapse just prior to the deposition of the 11.6 ± 0.03 Ma Rainier Mesa Tuff, and the third, and most extensive collapse, shortly after eruption of the 11.1 ± 0.3 Ma basalt.

Given the structural and geophysical models for the Crater Flat basin, cumulative throw across the Bare Mountain fault for this period was 1–2 km. Thus, the slip rate during what we consider the most active period of deformation (12–11 Ma) was on the order of 1–2 mm/yr. This rate is comparable to rates derived for currently active normal fault systems. For example, Martinez et al. (1998) record a modern-day, 5-mm/yr slip rate for the Wasatch fault based on GPS measurements. What is notable for the Bare Mountain fault is that the pulse

of high active rate persisted for 1 Ma or less. Since 11 Ma, it appears that the slip rate on Bare Mountain reduced one or two orders of magnitude. An average rate for the fault considering subsidence of southern Crater Flat and burial of the Little Cones is 0.06 mm/yr (Stamatakos et al., 1997). Paleoseismic estimates based on trenching data suggest a rate of less than 0.01 mm/yr (Klinger and Anderson, 1994).

IMPLICATIONS FOR SEISMIC AND FAULTING HAZARD ASSESSMENT

There are three important implications of these results to the current seismic hazard assessment for Yucca Mountain. First, the current seismic hazard assessment for Yucca Mountain (e.g., U.S. Geological Survey, 1998) assumes traditional planar-shaped domino-style faults. Estimates of the maximum magnitude earthquake (M_{max}) derived from empirical fault-scaling relationships (e.g., Wells and Coppersmith, 1994) thus consider fault planes that cut the entire thickness of the brittle crust (about 15 km in Nevada). In contrast, because our proposed structural models incorporate outer-arc extension of the hangingwall, faults observed at the surface do not necessarily cut through the entire seismogenic crust. Many displacement and tip downward. Hence, the effective area for fault rupture on faults that do not reach the base of the seismogenic crust is reduced. A seismic hazard assessment that incorporates faults that are assumed to cut the full crustal thickness may therefore overestimate the seismic hazard.

Second, we propose a structural link between the faults at Yucca Mountain and slip on the Bare Mountain fault. By inference, a large earthquake on the Bare Mountain fault could

lead to significant coseismic or postseismic deformation at Yucca Mountain. The Bare Mountain fault is the master fault of the basin. Crater Flat basin comprises the hangingwall. Faults at Yucca Mountain accommodate deformation of the hangingwall above the Bare Mountain fault. In this interpretation, the southward increase in fault slip simply reflects the change in dip on the Bare Mountain fault. As dip on the Bare Mountain fault steepens, it becomes less efficient at accommodating extension and thus requires more deformation of the hangingwall.

Third, we conclude that the majority of displacement presently observed across the Bare Mountain fault occurred in the Middle to Late Miocene, from 12 to 11 Ma. Since 11 Ma, the average slip rate on the fault has remained low, probably near the 0.06 mm/yr average rate we previously derived for the past 1 Ma, based on progressive burial of the Little Cones (Stamatakos et al., 1997). Thus, the recently proposed slip rates of 1–2 mm/yr for the fault based on GPS results (Wernicke et al., 1998) are either in error (e.g., Savage, 1998) or represent a geologically recent spike of increased crustal strain (e.g., Connor et al., 1999). There is simply not enough cumulative displacement across the fault remaining after the 12–11 Ma pulse to allow for the 1–2 mm/yr rate to be long lived.

IMPLICATIONS FOR VOLCANIC HAZARD ASSESSMENTS

The outer-arc extension model discussed in this paper illustrates how left- and right-stepping relay structures and vertical-axis block rotations developed in Crater Flat basin in response to progressive hangingwall deformation of the Bare Mountain fault. Our model does

not incorporate any significant periods of strike slip or transtensional tectonics. The major structural features of the Crater Flat basin that can localize ascending magma in the shallow crust were developed during a period of rapid extension and associated basaltic volcanism between about 12 and 11 Ma. Since 11 Ma, basaltic volcanism continued in the Crater Flat basin, but at significantly lower extension rates.

Although extension rates have slowed dramatically since 11 Ma, the same types of shallow crustal structures continued to localize ascending basaltic magma as during the period of rapid extension. For example, north-trending, left-stepping alignments in 3.8-Ma Crater Flat volcanoes and in 11.7 ± 0.3-Ma Solitario Canyon dikes were most likely localized along relay structures.

Based on the outer-arc extension model, continued extension of the Crater Flat basin at Plio-Quaternary rates permits generally northeast-trending normal faults and north-trending relay structures to accommodate the dilational strain associated with magma ascent. Relay and incipient relay structures intersect the proposed repository site at Yucca Mountain, in response to differential slip along the Solitario Canyon fault and nearby faults to the east (i.e., Ferrill et al., 1999b). Yucca Mountain thus contains structures that could potentially localize basaltic magma ascending during the current basin-scale stress regime. Spatial and temporal patterns of past volcanic activity shows the most likely location for a future eruption is within western Crater Flat basin—still significantly above background recurrence levels at the proposed repository site (e.g., Connor et al., 2000). The tectonic model presented herein attests the proposed Yucca Mountain repository site should not be subdivided from the rest

of Crater Flat basin into a zone of inactive or background level potential for future volcanic activity (e.g., Fridrich et al., 1999).

CONCLUSION

Detailed analyses of new and existing geological and geophysical data indicate the post- 15 Ma tectonic development of Crater Flat basin was primarily controlled by rapid phase extensional tectonics in the Middle to Late Miocene, 11–12 Ma. This pulse of Miocene deformation was manifest by fault slip on the Bare Mountain fault and concomitant deformation of the Crater Flat basin, which constitutes the hangingwall of the Bare Mountain fault. Deformation of the hangingwall was by outer-arc extension, producing faults in the hangingwall that tip downward in the crust. This deformation mechanism also produces a significant component of clockwise horizontal shear in the hangingwall. Because the dip of the Bare Mountain fault steepens from north to south, east-west extension of the basin required greater deformation of the hangingwall in southern Crater Flat. The geometric constraint is that steeper portions of the Bare Mountain fault were less efficient at accommodating extension of the crust.

The rapid phase of deformation and fault slip was coeval with the waning stages of pyroclastic volcanism of the southwestern Nevada volcanic field resulting in a thick accumulation of Rainier Mesa Tuff in a structurally controlled trough adjacent to the Bare Mountain fault. Rapid faulting also led to an overly steep and unstable topographic edifice of Paleozoic carbonate rocks at Bare Mountain. This edifice collapsed several times producing

an extensive and impressive volume of rock-avalanche megabreccia deposits in Crater Flat basin. Since this brief but intense period of deformation, tectonic activity in Crater Flat basin continues but at a significantly lower rate, comparable to the present tectonic activity.

This proposed tectonic model has several important implications to the seismic and volcanic hazard assessments for Yucca Mountain. First, our model suggests that many faults in the Crater Flat basin may not extend through the entire brittle crust. Hence, their potential for generating large-magnitude earthquakes may be overestimated in seismic hazard assessments that assume that all faults rupture the entire width of the seismogenic crust (e.g., U.S. Geological Survey, 1998). Second, our model shows that Bare Mountain fault controls much of the pattern of deformation observed across Crater Flat basin. Thus, slip on the Bare Mountain fault will likely trigger coseismic or postseismic faulting and fracturing at Yucca Mountain. Third, our model indicates that much of the post 15-Ma slip in the Bare Mountain fault occurred in a brief geologic interval between 12 and 11 Ma. Since that time, slip rates decreased by one to two orders of magnitude. Thus, it seems unlikely that rapid extension rates suggested by the recent GPS results of Wernicke et al. (1998) are significant, either because the GPS measurements are in error or because the recent accumulation of crustal deformation recorded by the GPS measurements is not sufficiently long-lived to build up a level of elastic strain to trigger a large earthquake. Fourth, the model shows that the pattern of past basaltic volcanic activity in the Crater Flat basin is well explained by basin structures. The model also establishes that Yucca Mountain lies within the Crater Flat structural domain and should not be subdivided from the rest of the Crater Flat basin in volcanic hazard assessments.

ACKNOWLEDGMENTS

The Center for Nuclear Waste Regulatory Analyses (CNWRA) of the Southwest Research Institute was established as a Federally Funded Research and Development Center by the Nuclear Regulatory Commission (NRC). The science documented in this paper is separate product of the CNWRA and in no way reflects the views or regulatory position of the NRC. We used OASIS montaj™ Version 4.2 and GM-SYS™ Version 4.0.4 for geophysical analyses. We thank Steve Lynton, Eugene Jarosewich, and James Luhr (Smithsonian Institution) for their expertise in the x-ray fluorescence analyses. Instrumental neutron activation analyses were conducted at the trace-element geochemistry laboratory at Washington University under the direction of Randy Korotev. $^{40}Ar/^{39}Ar$ analyses were completed by Chris Hall at the University of Michigan. Paleomagnetic analyses were performed at the University of Michigan by John Stamatakos. We thank Rob Van der Voo and colleagues for the hospitality of the Michigan facility. We also thank Annette Mandujano and Deborah Waiting for assistance with the figures and preparation of the manuscript. We thank Barbara Long and Alana Woods for their editorial reviews. Technical reviews by H. Lawrence McKague and John Russell greatly improved the quality of this manuscript.

APPENDIX 1. NEW $^{40}Ar/^{39}Ar$ DATE FOR CRATER FLAT PUMICE

Hand samples of 4–5 cm diameter subrounded to subangular pumice were collected from a 10-cm-thick matrix-poor interval of clast-supported lapilli 1.5 m below the basal contact

with 3.8 Ma basaltic lavas at 543960E 4066570N (NAD27, UTM Zone 11, Big Dune 7.5' quadrangle). Lapilli were cleaned with a wire brush to remove adhering material and washed with deionized water in an ultrasonic cleaner for cycles of 2–5 minutes until no surficial deposits remained. Lapilli were air dried and weathering rinds trimmed using a dull knife. Samples were coarsely crushed and feldspar phenocrysts separated from the matrix using standard heavy-mineral separation techniques. Neutron radiation was performed at the Phoenix-Ford Memorial Nuclear Reactor at the University of Michigan. Analytical procedures were identical to those described in Conway et al. (1997). All ages were calculated assuming 27.99 Ma for standard biotite FCT-3.

Twelve single feldspar crystals were analyzed using total-fusion analysis technique. Assuming an initial $^{40}Ar/^{39}Ar$ ratio of 295.5, and using the total-fusion analyses in Table A1, yields a date of 9.03 ± 0.30 Ma at two-sigma uncertainty. An isochron plot of these analyses (Figure A1) shows a robust linear array with a mean square of the weighted deviates at an acceptable value of 1.71. The initial $^{40}Ar/^{39}Ar$ ratio is within an analytical error of a 295.5 atmospheric ratio, indicating the total-fusion date accurately represents the age of the Crater Flat pumice.

APPENDIX 2. NEW MIOCENE BASALT $^{39}Ar/^{40}Ar$ AGES

At two sites in southern Crater Flat (text, Figure 1), hand samples of 1–2 kg of fresh basalt were collected for $^{39}Ar/^{40}Ar$ age analyses. Analyses were performed following the same procedures and techniques given in Appendix 1.

Sample analysis from the isochron analysis show robust linear arrays with mean square weighted deviate values less than 1. Apparent initial argon isotopic compositions are within an error of the atmospheric value of 295.5 (Table A2). In both samples, representative age-spectra diagrams (Figures A2A and A2B) and isotope correlation or isochron diagrams (Figures A2C and A2D) yield nearly identical isotopic $^{39}Ar/^{40}Ar$ dates of 11.2 ± 0.4 Ma (Table 2), an age consistent with the reversed polarity geomagnetic field during chron C5n.2r (Cande and Kent, 1992).

APPENDIX 3. GEOCHEMISTRY OF MIOCENE CRATER FLAT BASALT

Samples of Miocene basalt were collected from (a) lava outcrops in the Will Carr Hills, #2795-3 at 536790E 4063380N and #72396-1 at 534680E 4066450N (NAD27, UTM Zone 11, Big Dune 7.5' quadrangle); (2) dike outcrops north of Solitario Canyon #42396-2 at 546850E 4082010N (NAD27, UTM Zone 11, Pinnacles Ridge 7.5' quadrangle); and (3) core from 1193 feet in drill hole USW VH-2 #VH2-1193 at 537900E 4072950N (NAD27, UTM Zone 11, Crater Flat 7.5' quadrangle).

After cleaning and trimming, 25-g sample splits were pulverized in an alumina-ceramic shatterbox to <0.075 mm diameter. Sample preparation and x-ray fluorescence (XRF) analyses were conducted by Steven Lynton, directed by Eugene Jarosewich and James Luhr at the Smithsonian Institution. Major element XRF analyses fused 0.6 g of rock powder with 6 g of lithium metaborate flux, which is weighed after fusion to determine loss on ignition.

Trace XRF analyses mixed 1 g of rock powder with 5 g of cellulose binder, which was pressed into a disk for beam analysis (Table A3).

Instrumental neutron activation (INA) analyses were conducted in the trace-element geochemistry laboratory at Washington University under the direction of Randy Korotev. Standard INA radioanalytical techniques were used, as outlined in Korotev (1991). Rock powder splits (0.25 g) were irradiated for 6 hr at 1 MW reactor power. Samples were radioassayed three times at 6–7 days, 7–11 days, and >28 days following irradiation (Table A3).

Analytical precision for each technique was determined by replicate analyses of samples and internal calibration checks with standard reference materials. Analytical accuracy was determined by analysis of USGS reference standard BHVO–1 (Hawaiian basalt) and comparison with generally accepted element abundances (e.g., Govindaraju, 1994). Analyzed values for BHVO–1 are all within analytical precision of reference values for this standard. Uncertainties in Table A3 represent the precision and accuracy of the analyses.

APPENDIX 4. PALEOMAGNETISM OF MIOCENE BASALT AND MEGABRECCIA

Miocene Basalt

At six sites (text, Figure 1), eight cores of basalts per site were collected. Samples were drilled in the field using a gasoline-powered coring device and oriented with a sun compass. Bedding was determined from triangulation and measurements of layering.

Characteristic magnetizations were isolated from progressive thermal demagnetization, consisting of 9–15 heating steps to a peak temperature of 585 °C, and progressive alternating field (af) demagnetization, consisting of 10–15 steps to a peak af of 160 mT. Thermal demagnetizations were accomplished using a standard paleomagnetic furnace with a maximum rest field of 10 nT. A three-axis cryogenic magnetometer in the magnetically shielded facility at the University of Michigan was used to make all magnetic measurements. Peak ambient field in the shielded room is less than 600 nT. Magnetic components were determined from visual inspection of the linear portions of the vector end-point diagrams. Component directions were calculated from a least square fit of the observed linear trajectories (Kirschvink, 1980). Sample directions were combined to form site means using vector addition and giving unit weight to each sample direction. Statistical parameters were calculated according to Fisher (1953).

Intensities of the natural remanent magnetization (NRM) ranged between 1.0 and 5.5 A/m with an average of 4.5 A/m. Thermal and alternating field demagnetization revealed two components of magnetization with discrete to slightly overlapping unblocking temperature spectra (Figure A3A and A3B). A secondary direction with northerly declinations and moderately down inclinations was first removed with an unblocking temperature range between 25 °C and 200 °C and af up to 10 mT. The characteristic remanent magnetization (ChRM), with south or south-southeast declinations and moderately up inclinations, was isolated with a distributed unblocking temperature spectrum between 200 °C and 580 °C and alternating fields between 10 and 160 mT.

Samples for all sites yielded well defined ChRM directions (Figure A4A and A4B and Table A4). Mean directions for the six sites were optimally grouped in stratigraphic coordinates as shown by the incremental tilt test [Figure A4C, based on McElhinny, (1964)]. Site mean directions and the grand mean direction, after tilt correction, fall near the expected Miocene reference direction (Figure A4B) derived from the Miocene reference pole of Hagstrum et al. (1987). The amount of vertical- or inclined-axis rotation (Table A4) was computed following the method of Demarest (1983), using a reference declination of 357°, $\Delta D = 3.7$. Rotations for the six sites range between $-5.0° \pm 13.4°$ and $25.2 \pm 11.4°$. The formation mean shows a small clockwise rotation of $12.3° \pm 10.3°$.

Megabreccia

For the megabreccias, 16–18 samples per site were collected from 5 sites (Figure 1), eight samples from breccia clasts, and 8–10 samples from the surrounding matrix. Samples were drilled in the field using a gasoline-powered coring device and oriented with a magnetic compass. There were no obvious markers of paleohorizontal, and thus we assumed a uniform northeast tilt of 10° for all sites based on the post 10 Ma tilting of the rocks in southern Crater Flat proposed by Fridrich (1999). ChRM were isolated from progressive thermal demagnetization, consisting of 9–12 heating steps to a peak temperature of 550°C. In a pilot sample, alternating field demagnetization produced spurious and erratic demagnetization behavior and thus this technique was not used for further demagnetization of the megabreccia

samples. Thermal demagnetization and identification of the ChRM follow the description given previously for the Miocene basalt samples.

Intensities of the NRM ranged between 100.0 and 0.01 mA/m, with an average of 3.1 mA/m. Average NRM intensity for the matrix samples was 6.7 mA/m compared to an average of 1.1 mA/m for the clasts. Thermal demagnetization revealed a single component of magnetization with distributed unblocking temperature spectra between 100 °C and 550° C (Figures A3C and A3D). ChRM directions are north and moderately down or antipodal south and moderately up (Figures A4D and A4E and Table A4). Intensity was the most important controlling factor in whether the sample produced a coherent ChRM and, thus, most of the reliable ChRM directions were derived from the matrix material. Samples with NRM intensities below 0.1 mA/m were too weak to resolve reliable ChRM directions.

Mean directions for the five sites and the grand mean direction, before or after the small tilt correction, are near the expected Miocene reference direction (Figures A4D and A4E) derived from the Miocene reference pole of Hagstrum et al. (1987). These results indicate that the megabreccias were remagnetized following their emplacement in the Miocene. We suggest that remagnetization most likely occurred during cementation based on the observation that most reliable ChRM directions come from matrix samples. In addition, the presence of a two-polarity ChRM suggests acquisition times of the remagnetization over at least one reversal of the Earth's magnetic field. Following the method used for the basalt rocks, the amount of vertical- or inclined-axis rotation (Table A4) for the five sites is within the errors; the range is between $-8.9° \pm 35.3°$ and $12.0 \pm 26.6°$. The grand mean yields a small clockwise rotation of $2.9° \pm 9.0°$ that also is not statistically different from 0.

FIGURE CAPTIONS

Figure 1. Generalized geologic map of Crater Flat, Nevada, including Bare Mountain and Yucca Mountain. Map sources are Frizzell and Schulters (1990), Monsen et al. (1992), Langenheim (1995), and Swadley and Carr (1987). Insets provide the location of the map and relevant regional features on a digital elevation model of the southwestern United States and an enlarged map of the Will Carr Hills showing sampling locations for paleomagnetic and $^{40}Ar/^{39}Ar$ analyses.

Figure 2. Generalized stratigraphic columns of the stratigraphy of Bare Mountain and Crater Flat basin. Sources are [1]Monsen et al. (1992); [2]Sawyer et al. (1994); [3]Paces et al. (1993); [4]Heizler et al. (1999); [5]Quade et al. (1995); [6]Fleck et al. (1996),[7]Stamatakos et al. (1997); [8]Carr and Parrish, 1985; [9]this paper; and [10]Smith et al. (1997). Fleck et al. (1996) report an age range of 0.97–1.04 Ma for Quaternary Crater Flat, although this age range does not agree with reversed polarity remanent magnetization. Stamatakos et al. (1997) suggest this basalt erupted during chron C1r.1r or C1r.2r of the geomagnetic time scale (Cande and Kent, 1992; Izett and Obradovich, 1994) giving an age of 0.78–0.97 Ma or 1.10–1.75 Ma, respectively.

Figure 3. (A) and (B) are non annotated and annotated photo mosaics of southern Crater Flat and the Will Carr Hills. View is looking west-northwest toward Bare Mountain. (C) and (D)

are photographs of two outcrop exposures of the megabreccia on the Will Carr Hills. (E) is a photomicrograph showing typical petrography of the megabreccia.

Figure 4. (A) Stratigraphic sections of USW VH-2 and USW VH-1 boreholes based on lithologic logs and stratigraphic descriptions given by Carr (1982) and Carr and Parrish (1985). Insert shows details of megabreccias MB2, MB3, and MB4. (B) Photograph of megabreccia 9 m above the basal contact in USW VH-2 core, 351-meter depth. (C) Plain-light photomicrograph showing petrography of the megabreccia for comparison to the photomicrograph from an outcrop sample in the Will Carr Hills (Figure 3D). (D) A 3-cm thick section of sheared and deformed sediment between the 11.3 ± 0.3 Ma basalt and overlying megabreccia.

Figure 5. (A) Complete Bouger anomaly (gravity) map encompassing Crater Flat basin. Colored contour intervals are 2 mGal. Data are from numerous data source compiled in Ponce and Oliver (1995). Maps were generated using OASIS Montaj™ Version 4.2 software. (B) Magnetic anomaly map based on aeromagnetic data of Kane and Bracken (1983). Faults on both (A) and (B) are from digital coverage of Frizzell and Schulters (1990). Maps are projected in UTM coordinates, Zone 11.

Figure 6. Summary map showing the amount of vertical-axis rotation calculated for sites across Bare Mountain, Crater Flat, and Yucca Mountain based on paleomagnetic data. References are [1]Connor et al. (unpublished data), [2]Champion (1995), [3]this paper

(Appendix 4), [4]Fridrich et al. (1999), [5]Hudson et al. (1994), [6]Rosenbaum et al. (1991), and [7]Stamatakos et al. (1998). Data are plotted on a digital elevation model projected in UTM coordinates, Zone 11. Faults are from digital coverage of Frizzell and Schulters (1990).

Figure 7. Plot of the amount of vertical-axis rotation recorded by paleomagnetic data in rocks from the Will Carr Hills. The unit-mean rotations were simple averages of the site-mean rotations. Uncertainties for the rotations were calculated as standard errors (i.e., the square root of the sum of the squares of the site-mean errors, divided by the number of sites). Uncertainties in the age estimates are from the uncertainties reported for the radiometric dates. For the megabreccia, we assume magnetization was acquired soon after deposition (Appendix 4).

Figure 8. Conceptual diagram of extensional deformation showing development of vertical-axis rotations in deforming hangingwall blocks juxtaposed with rigid footwall blocks along faults with large throw gradients, for (A) southward increasing and (B) northward increasing fault displacements.

Figure 9. (A) The Iron Ridge and (B) Southern Solitario Canyon relay systems from geological maps of Day et al. (1998) and Swadley and Carr (1987). ΔR and associate 95% confidence intervals based on the paleomagnetic results for the Tiva Canyon sites located on these relay structures (Rosenbaum et al., 1991; Hudson et al., 1994).

Figure 10. East-west cross-section through Crater Flat basin modified from Ferrill et al. (1996a). The line of this cross section is shown in Figure 1 (A-A').

Figure 11. Conceptual diagram illustrating hangingwall deformation and clockwise vertical-axis rotation above a listric normal fault. Overall extension of the basin is uniform. Differential deformation of the hangingwall is produced by the southward increase in dip of the master fault. (A) Model showing that constant bed-length and bed-thickness deformation requires layer-parallel shear in the hangingwall (see shear profile). (B) Model showing that the southward-increasing outer-arc extension in the hangingwall producing clockwise rotations of the fault blocks.

Figure 12. (A) Gravity and (B) magnetic models depicting thickened Bullfrog and Rainier Mesa tuffs. Gravity data used in (A) was obtained from geophysical data repository at Lawrence Berkeley Laboratory (Ponce and Oliver, 1995). Magnetic profile used in (B) was extracted from the aeromagnetic map grid (Figure 5B). Models were generated using GM-SYS™ Version 4.04 software.

Figure A1. Isochron plot of single-crystal total fusion $^{40}Ar/^{39}Ar$ analyses of Crater Flat pumice sample 72696-5. MSWD = 1.71, n = 12, t = 9.24 ± 0.87, +/- $^{40}Ar/^{36}Ar_i$ = 294.3 ± 5.5.

Figure A2. $^{40}Ar/^{39}Ar$ age determinations for basalt samples from the Will Carr Hills, Nevada. (A) and (B) are $^{40}Ar/^{39}Ar$ age spectra from step-wise heating analysis. Boxes are ± 1 sigma.

(C) and (D) are isochron plots of single-crystal total fusion analyses, with error ellipses at ± 1 sigma. (E) and (F) are enlargements of the isochron plots.

Figure A3. Representative vector end-point diagrams showing thermal and alternating field demagnetization of samples from (A) and (B) the 11.1 ± 0.3 Ma basalt and (C) and (D) megabreccia samples from the Will Carr Hills. Open and closed symbols are projections onto the vertical and horizontal planes. Thermal demagnetization steps are in °C, alternating field demagnetization steps are in mT.

Figure A4. Summary of paleomagnetic site-mean directions from 11.1 ± 0.3 Ma basalt and megabreccia samples from the Will Carr Hills. (A) and (B) are equal angle projections before and after tilt correction of 11.2 ± 0.3 Ma basalt. Stars show the orientations of the normal and reversed-polarity Miocene reference direction (Hagstrum et al., 1987). (C) Plot of the incremental fold test (McElhinny, 1964) showing an increase in the precision parameter, kappa (k), as a function of untilting. (D) and (E) are equal angle projections before and after tilt correction of megabreccia.

REFERENCES CITED

Ackermann, H. D, Mooney, W. D., Snyder, D. B., and Sutton, V. D., 1988, Preliminary interpretation of seismic-refraction and gravity studies west of Yucca Mountain, Nevada, and California, *in* Carr, M. D., and Yount, J. C., eds., Geologic and hydrologic investigation of a potential nuclear waste disposal site at Yucca Mountain, southern Nevada: U.S. Geological Survey Bulletin 1790, p. 23–34.

Armstrong, R. L., 1968, Sevier orogenic belt in Nevada and Utah: Geological Society of America Bulletin, v. 79, p. 439–458.

Axen, G. J., Taylor, W. J., and Bartlet, J. M., 1993, Space-time patterns and tectonic controls of tertiary extension and magmatism in the Great Basin of the western United States: Geological Society of America Bulletin, v. 105, p. 56–76.

Baldwin J. M., and Jahren, C. E., 1982, Magnetic properties of drill core and surface samples from the Calico Hills area, Nye County, Nevada: U.S. Geological Survey Open-File Report 85-536, 27 p.

Blakely, R. J., Morin, R. L., McKee, E. H., Schmidt, K. M., Langenheim, V. E., and Dixon, G. L., 1998, Three-dimensional model of Paleozoic basement beneath Amargosa Desert

and Pahrump Valley, California and Nevada: Implications for tectonic evolution and water resources: U.S. Geological Survey Open-File Report 98-496, 29 p.

Blakely, R. J., Jachens, R. C., Calzia, J. P., and Langenheim, V. E., 1999, Cenozoic basins of the Death Valley extended terrane as reflected in regional-scale gravity anomalies, *in* Wright, L. A., and Troxel, B. W., eds., Cenozoic basins of the Death Valley region: Geological Society of America Special Paper 333, p. 1–16.

Brocher, T. M., Hunter, W. C., and Langenheim, V. E., 1998, Implications of seismic reflection and potential field geophysical data on the structural framework of the Yucca Mountain-Crater Flat region, Nevada: Geological Society of America Bulletin, v. 110, p. 947–971.

Byers, F. M., Jr., Carr, W. J., Orkild, P. P., Quinlivan, W. D., and Sargent, K. A., 1976a, Volcanic suites and related cauldrons of the Timber Mountain-Oasis Valley caldera complex: U.S. Geological Survey Professional Paper 919, 70 p.

Byers, F. M., Jr., Carr, W. J., Christiansen, R. L., Lipman, P. W., Orklid, P. P., and Quinlivan, W. D., 1976b, Geologic Map of the Timber Mountain caldera area, Nye County, Nevada: U.S. Geological Survey Miscellaneous Investigation Series Map I–891, **SCALE**.

Cande, S. C., and Kent, D. V., 1992, A new geomagnetic polarity time scale for the Late Cretaceous and Cenozoic: Journal of Geophysical Research, v. 97, p. 13,917–13,951.

Carey, S., and Sparks, R. S. J., 1986, Quantitative models of the fallout and dispersal of tephra from volcanic eruption columns: Bulletin of Volcanology, v. 48, p. 109–125.

Carr, W. J., 1982, Volcano-tectonic history of Crater Flat, southwestern Nevada, as suggested by new evidence from drill hole USW VH-1: U.S. Geological Survey Open-File Report 82-457, 23 p.

Carr, W. J., 1984, Regional structural setting of Yucca Mountain, southwestern Nevada, and late Cenozoic rates of tectonic activity in part of the Southwestern Great Basin, Nevada and California: U.S. Geological Survey Open-File Report 84-854, 109 p.

Carr, W. J., 1990, Styles of extension in the Nevada test site region, southern Walker Lane belt: An integrated volcano-tectonic and detachment fault model: Geological Society of America Memoir, v. 176, p. 283–303.

Carr, W. J., and Parrish, L. D., 1985, Geology of drill hole USW VH-2 and structure of Crater Flat, southwestern Nevada: U.S. Geological Survey Open-File Report 85-475, 41 p.

Carr, W. J., Wadell, S. J., Vick, G. S., Stock, J. M., Monsen, S. A., Harris, A. G., Cork, B. W., and Byers, F. M., Jr., 1986, Geology of drill hole UE 25p#1: A test hole into pre-Tertiary rocks near Yucca Mountain, southern Nevada: U.S. Geological Survey Open-File Report 86-175, 87 p.

Champion, D. E., 1995, Volcanic episodes near Yucca Mountain as determined by paleomagnetic studies at Lathrop Wells, Crater Flat, and Sleeping Butte, Nevada: U.S. Geological Survey Open-File Report 95-563, 8 p.

Christiansen, R. L., and Lipman, P., 1965, Geologic Map of the Topopah Spring NW Quadrangle, Nye County, Nevada: U.S. Geological Survey Geological Quadrangle Map GQ–444, 1:24,000.

Christiansen, R. L., Lipman, P. W., Carr, W. J., Byers, F. M., Jr., Orkild, P. P., and Sargent, K. A., 1977, Timber Mountain-Oasis Valley caldera complex of southern Nevada: Geological Society of America Bulletin, v. 88, p. 943–959.

Connor, C. B., Lane-Magsino, S., Stamatakos, J. A., Martin, R. H., La Femina, P. C., Hill, B. E., and Lieber, S., 1997, Magnetic surveys help reassess volcanic hazards at Yucca Mountain, Nevada: Eos (Transactions of the American Geophysical Union), v. 78, p. 73–78.

Connor, C. B., Stamatakos, J. A., Ferrill, D. A., and Hill, B. E., 1999, Comment on detecting strain in the Yucca Mountain Area, Nevada: Science, v. 282, p. 1007b.

Connor, C. B., Stamatakos, J. A., Ferrill, D. A., Hill, B. E., Ofoegbu, G. I., Conway, F. M., Sagar, B., and Trapp, J., 2000, Geologic factors controlling patterns of small-volume basaltic volcanism: Application to a volcanic hazards assessment at Yucca Mountain, Nevada: Journal of Geophysical Research, v. 105, p. 417–432.

Conway, M. F., Ferrill, D. A., Hall, C. M., Morris, A. P., Stamatakos, J. A., Connor, C. B., Halliday, A. N., Condit, C., 1997, Timing of basaltic volcanism along the Mesa Butte fault in the San Francisco volcanic field, Arizona, from $^{40}Ar/^{39}Ar$ dates: Implications for longevity of cinder cone alignments: Journal of Geophysical Research, v. 102, p. 815–824.

Craig, R. W., Reed, R. L., and Spengler, R. W., 1983, Geohydrologic Data for Test Well USW H-6, Yucca Mountain area, Nye County, Nevada: U.S. Geological Survey Open-File Report 83-856, 35 p.

Crowe, B. M., 1986, Volcanic hazard assessment for disposal of high-level radioactive waste: Active tectonics: Impact on society: Geophysics Study Committee, National Research Council: Washington, DC, National Academy Press, p. 247–260.

Crowe, B. M., Johnson, M. E., and Beckman, R. J., 1982, Calculation of the probability of volcanic disruption of a high-level nuclear waste repository within southern Nevada, USA: Radioactive Waste Management and the Nuclear Fuel Cycle, v. 3, p. 167–190.

Crowe, B. M., Vaniman, D. T., and Carr, W. J., 1983, Status of volcanic hazard studies for the Nevada nuclear waste storage investigations: Los Alamos National Laboratory Report LA–9325–MS, 101 p.

Crowe, B., Perry, F., Geissman, J., McFadden, L., Wells, S., Murrell, M., Poths, J., Valentine, G. A., Bowker, L., and Finnegan, K., 1995, Status of volcanism for the Yucca Mountain site characterization project: Los Alamos National Laboratory Report 12908–MS, p. 2-18 to 2-21.

Day, W. C., Potter, C. J., Sweetkind, D. S., Dickerson, R. P., and San Juan, C. A., 1997, Bedrock geologic map of the central block area, Yucca Mountain: U.S. Geological Survey Miscellaneous Investigations Series Map I–2601, scale 1:6000.

Day, W. C., Dickerson, R. P., Potter, C. J., Sweetkind, D. S., San Juan, C. A., Drake, R. M., II, and Fridrich, C. J., 1998, Geologic map of the Yucca Mountain area, Nye County, Nevada: U.S. Geological Survey Geological Investigations Series I–2627, scale 1:24,000.

Demarest, H. H., 1983, Error analysis for the determination of tectonic rotations from paleomagnetic data: Journal of Geophysical Research, v. 88, p. 4,321–4,328.

Dula, W. F., Jr., 1990, Geometric models of listric normal faults and rollover folds: American Association of Petroleum Geologists Bulletin, v. 75, p. 1,609–1,625.

Ekren, E. B., Anderson, R. E., Rogers, C. L., and Noble, D. C., 1971, Geology of Northern Nellis Air Force Base Bombing and Gunnery Range, Nye County, Nevada: U.S. Geological Survey Professional Paper 651.

Faulds, J. E., Bell, J. W., Feuerbach, D. L., and Ramelli, A. R., 1994, Geologic map of the Crater Flat area, Nevada: Nevada Bureau of Mines and Geology Map 101, scale 1:24,000.

Ferrill, D. A., and Morris, A.P. ,1997, Geometric considerations of deformation above curved normal faults and salt evacuation surfaces: The Leading Edge, v. 16, p. 1129–1133.

Ferrill, D. A., Stirewalt, G. L., Henderson, D. B., Stamatakos, J. A., Spivey, K. H., and Wernicke, B. P., 1996a, Faulting in the Yucca Mountain region, critical review and analyses of tectonic data from the Central Basin and Range: Nuclear Regulatory Commission, NUREG/CR–6401, 105 p.

Ferrill, D. A., Stamatakos, J. A., Jones, S. M., Rahe, B., McKague, H. L., Martin, R. H., and Morris, A. P., 1996b, Quaternary slip history of the Bare Mountain fault (Nevada) from the morphology and distribution of alluvial fan deposits: Geology, v. 24, p. 559–562.

Ferrill, D. A., Stamatakos, J. A., and McKague, H. L., 1997, Quaternary slip history of the Bare Mountain Fault (Nevada) from the morphology and distribution of alluvial fan deposits: Reply: Geology, v. 25, p. 190.

Ferrill, D. A., Morris, A. P., Jones, S. M., and Stamatakos, J. A., 1998, Extensional layer-parallel shear and normal faulting: Journal of Structural Geology, v. 20, p. 355–362.

Ferrill, D. A., Stamatakos, J. A., and Sims, D., 1999a, Normal fault corrugation: Implications for growth and seismicity of active normal faults: Journal of Structural Geology, v. 21, p. 1027–1038.

Ferrill, D. A., Winterle, J., Wittmeyer, G., Sims, D., Colton, S., Armstrong, A., and Morris, A. P., 1999b, Stressed rock strains groundwater at Yucca Mountain, Nevada: GSA Today, vol. 9, No. 5, p. 1–8.

Fisher, R. A., 1953, Dispersion on a sphere: Proceedings of the Royal Society of London, Ser. A, v. 217, p. 295–305.

Fleck, R. J., Turrin, B. D., Sawyer, D. A., Warren, R. G., Champion, D. E., Hudson, M. R., and Minor, S. A., 1996, Age and character of basaltic rocks of the Yucca Mountain region, southern Nevada: Journal of Geophysical Research, v. 101, p. 8205–8227.

Fridrich, C. J., 1999, Tectonic evolution of the Crater Flat basin, Yucca Mountain region, Nevada, Cenozoic basins of the Death Valley region: *in* Wright, L. A., and Troxel, B. W., eds., Cenozoic basins of the Death Valley region: Geological Society of America Special Paper 333, p. 169–196.

Fridrich, C. J., Whitney, J. W., Hudson, M. R., and Crow, B. M., 1999, Late Cenozoic extension, vertical-axis rotation, and volcanism in the Crater Flat basin, southwest Nevada, *in* Wright, L. A., and Troxel, B. W., eds., Cenozoic basins of the Death Valley region: Geological Society of America Special Paper 333, p. 197–212.

Frizzell, V. A., and Shulters, J., 1990, Geologic map of the Nevada test site, southern Nevada: U.S. Geological Survey Miscellaneous Investigations Series Map I-2046, scale 1:100,000.

Geomatrix, 1996, Probabilistic volcanic hazards analysis for Yucca Mountain, Nevada, San Francisco, CA, Geomatrix Consultants, Report BA0000000-1717-2200-00082, Rev. 0, 333 p.

Gillett, S. L., and Van Alstine, D. R., 1982, Remagnetization and tectonic rotation of Upper Precambrian and Lower Paleozoic strata from the Desert Range, southern Nevada: Journal of Geophysical Research, v. 87, p. 10,929–10,953.

Govindaraju, K., 1994, Compilation of working values and descriptions for 383 geostandards: Geostandards Newsletter, v. 118, p. 1–158.

Groshong, R. H., Jr., 1989, Half-graben structures: Balanced models of extensional fault-bend folds: Bulletin of the Geological Society of America, v. 101, p. 96–105.

Groshong, R. H., Jr., 1990, Unique determination of normal fault shape from hanging-wall bed geometry in detached half grabens: Eclogae Geologicae Helvetiae, v. 83, p. 455–471.

Hagstrum, J. T., Sawlan, M. G., Hausback, B. P., Smith, J. G., and Grommé, C. S., 1987, Miocene paleomagnetism and tectonic setting of the Baja California Peninsula, Mexico: Journal of Geophysical Research, v. 92, p. 2627–2639.

Hamilton, W. B., 1988, Detachment faulting in the Death Valley region, California and Nevada, *in* Carr, M. D., and Yount, J. C., eds., Geologic and hydrologic investigations of a potential nuclear waste disposal site at Yucca Mountain, southern Nevada: U.S. Geological Survey Bulletin, v. 1790, p. 51–85.

Hardyman, R. F., and Oldow, J. S., 1991, Tertiary tectonic framework and Cenozoic history of the central Walker Lane, Nevada, *in* Raines, G. L., Lisle, R. E., Schafer, R. W., and Wilkinson, W. H., eds., Geology and ore deposits of the great basin: Geological Society of Nevada Symposium Proceedings 1, p. 279–301.

Heizler, M. T., Perry, F. V., Crowe, B. M., Peters, L., and Appelt, R., 1999, The age of Lathrop Wells volcanic center: An $^{40}Ar/^{39}Ar$ dating investigation: Journal of Geophysical Research, v. 104, p. 767–804.

Ho, C.-H., 1992, Risk assessment for the Yucca Mountain high-level nuclear waste repository site: Estimation of volcanic disruption: Mathematical Geology, v. 24, p. 347–364.

Hoisch, T. D., Heizler, M. T., and Zartman, R. E., 1997, Timing of detachment faulting in the Bullfrog Hills and Bare Mountain area, southwestern Nevada: Inferences from $^{40}Ar/^{39}Ar$, K-Ar, U-Pb, and fission track thermochronology: Journal of Geophysical Research, v. 102, p. 2815–2833.

Holm, D. K., Geissman, J. W., and Wernicke, B., 1993, Tilt and rotation of the footwall of a major normal fault system, paleomagnetism of the Black Mountains, Death Valley extended terrain, California: Geological Society of America Bulletin, v. 105, p. 1373–1387.

Hudson, M. R., 1992, Paleomagnetic data bearing on the origin of arcuate structures in the French Peak-Massachusetts Mountains area of southern Nevada: Geological Society of America Bulletin, v. 104, p. 581–594.

Hudson, M. R., Sawyer, D. A., and Warren, R. G., 1994, Paleomagnetism and rotation constraints for the Miocene southwestern Nevada volcanic field: Tectonics, v. 13, p. 258–277.

Hudson, M. R., Minor, S. A., and Fridrich, C. J., 1996, The distribution, timing, and character of steep-axis rotations in a broad zone of dextral shear in southwestern Nevada: Geological Society of America Abstracts with Programs, v. 28, p. A451.

Izet, G. A., and Obradovich, J. D., 1994, $^{40}Ar/^{39}Ar$ age constraints on the Jaramillo normal subchron and Matuyama geomagnetic boundary: Journal of Geophysical Research, v. 99, p. 2925–2934.

Kane, M. F., and Bracken, R. E., 1983, Aeromagnetic map of Yucca Mountain and surrounding regions, southwest Nevada: U.S. Geological Survey Open-File Report 83-616, 19 p.

Kirschvink, J. L., 1980, The least-squares line and plane and the analysis of paleomagnetic data: Geophysical Journal of the Royal Astronomical Society, v. 62, p. 699–718.

Klinger, R. E., and Anderson, L. W., 1994, Topographic profiles and their implications for late Quaternary activity on the Bare Mountain fault, Nye County, Nevada: Geological Society of America Abstracts with Programs, v. 26, p. A63.

Korotev, R. L., 1991, Geochemical stratigraphy of two regolith cores from the Central Highlands of the Moon, *in* Sharpton, V. L., and Ryder, G., eds., Proceedings of the 21st Lunar and Planetary Science Conference, Houston, TX: Lunar and Planetary Institute, p. 229–289.

Langenheim, V. E., 1995, Magnetic and gravity studies of buried volcanic centers in the Amargosa Desert and Crater Flat, southwest Nevada: U.S. Geological Survey Open-File Report 95-564, 39 p.

Langenheim, V. E., and Ponce, D. A., 1995, Ground magnetic studies along a regional seismic-reflection profile across Bare Mountain, Crater Flat and Yucca Mountain, Nevada: U.S. Geological Survey Open-File Report 95-834.

Lipman, P. W., and Christiansen, R. L., 1964, Zonal features of an ash-flow sheet in the Piapi Canyon formation, southern Nevada: U.S. Geological Survey Professional Paper 501-B, p. B74–B78.

Magsino, S. L., Connor, C. B., Hill, B. E., Stamatakos, J. A., La Femina, P. L., Sims, D. A., and Martin, R. H., 1998, CNWRA ground magnetic surveys in the Yucca Mountain region, Nevada (1996–1997), San Antonio, TX: Center for Nuclear Waste Regulatory Analyses, CNWRA 98-001, 31 p.

Maldonado, F., 1990, Structural geology of the upper plate of the Bullfrog Hills detachment fault system, southern Nevada: Geological Society of America Bulletin, v. 102, p. 992–1,006.

Maldonado, F., and Koether, S. L., 1983, Stratigraphy, structure, and some petrographic features of Tertiary volcanic rocks at the USW G-2 Drill Hole, Yucca Mountain, Nye County, Nevada: U.S. Geological Survey Open-File Report 83-732, 83 p.

Martinez, L., Meertens, C. M., and Smith, R. B., 1998, Anomalous intraplate deformation of the Basin and Range-Rocky Mountain transition from initial GPS measurements: Geophysical Research Letters, v. 24, p. 2741–2744.

McCafferty, A. E., and Grauch, V. S. J.,1997, Aeromagnetic and gravity anomaly maps of the southwestern Nevada volcanic field, Nevada and California: U.S. Geological Survey Geophysical Investigations Map GP-1015, scale 1:250,000.

McElhinny, M., 1964, Statistical significance of the fold test in paleomagnetism: Geophysical Journal, v. 8, p. 338–340.

McKay, E. J., and Sargent, K. A., 1970, Geologic map of the Lathrop Wells Quadrangle, Nye County, Nevada, Reston, VA: U.S. Geological Survey Map GQ–883, scale 1:24,000.

Minor, S. A., Hudson, M. R., and Fridrich, C. J., 1997. Fault-slip, paleomagnetic, and paleostress analyses bearing on the Neogene tectonic evolution of northern Crater Flat basin, Nevada: U.S. Geological Survey Open-File Report 97-285.

Monsen, S. A., Carr, M. D., Reheis, M. C., and Orkild, P. A., 1992, Geologic map of Bare Mountain, Nye County, Nevada: U.S. Geological Survey Miscellaneous Investigations Series Map I–2201, scale 1:24,000.

Morris, A. P., and Ferrill, D. A., 1999, Constant thickness deformation above curved normal faults: Journal of Structural Geology, v. 21, p. 67–83.

Morris, A. P., Ferrill, D. A., and Henderson, D. B., 1996, Slip-tendency analysis and fault reactivation: Geology, v. 24, p. 275–278.

National Research Council, 1995, Technical Bases for Yucca Mountain Standards: Washington, DC: National Academy Press, 104273.

Nelson, M. R., and Jones, C. H., 1987, Paleomagnetism and crustal rotations along a shear zone, Las Vegas range, southern Nevada: Tectonics, v. 6, p. 13–33.

Oldow, J. S., Kohler, G., and Donelick, R. A., 1994, Late Cenozoic extensional transfer in the Walker Lane strike-slip belt, Nevada: Geology, v. 22, p. 637–640.

O'Leary, D. W., 1996, Synthesis of tectonic models for the Yucca Mountain area, *in* Whitney, J. W., ed., Seismotectonic framework and characterization of faulting at Yucca Mountain, Nevada: U.S. Geological Survey Report to the U.S. Department of Energy, Milestone 3GSH100M, p. 8-1–8-153.

Oliver, H. W., and Fox, K. F., 1993, Structure of Crater Flat and Yucca Mountain, southeastern Nevada, as interpreted from gravity data, *in* Proceedings, Fourth Annual International Conference, Las Vegas, Nevada, 2: American Nuclear Society, p. 1812–1817.

Oliver, H. W., and **x** others, 1995, Magnetic investigations: Major results of geophysical investigations at Yucca Mountain and vicinity, southern Nevada: U.S. Geological Survey Open-File Report 95-74, p. 55–72.

Paces, J. B., Taylor, E. M., and Bush, C. A., 1993, Late Quaternary history and uranium isotopic compositions of ground water discharge deposits, Crater Flat, Nevada:

Proceedings of the Fourth International High-level Radioactive Waste Management Conference, v. 2, p. 1573–1580.

Peacock, D. C. P., and Sanderson, D. J., 1994, Geometry and development of relay ramps in normal fault systems: American Association of Petroleum Geologists Bulletin, v. 78, p. 147–165.

Peterson, F. R., Bell, J. W., Dorn, R. I., Ramelli, A. R., and Ku, T.-L., 1995, Late Quaternary geomorphology and soils in Crater Flat, Yucca Mountain area, southern Nevada: Geological Society of America Bulletin, v. 107, p. 379–395.

Plume, R. W., and La Camera, R. J., 1996, Hydrogeology of rocks penetrated by Test Well JF-3, Jackass Flats, Nye County, Nevada: U.S. Geological Survey Open-File Report 95-4245, 27 p.

Ponce, D. A., and Oliver, H. W., 1995, Gravity investigations: Major results of geophysical investigations at Yucca Mountain and vicinity, southern Nevada: U.S. Geological Survey Open-File Report 95–74, p. 33–54.

Quade, J., Mifflin, M. D., Pratt, W. L., McCoy, W., and Burckle, L., 1995, Fossil spring deposits in the southern Great Basin and their implications for changes in water-table levels

near Yucca Mountain, Nevada, during Quaternary time: Geological Society of America Bulletin, v. 107, no. 2, p. 213–230.

Reheis, M. C., 1988, Preliminary study of Quaternary faulting on the east side of Bare Mountain, Nye County, Nevada, *in* Carr, M. D., and Yount, J. C., eds., Geologic and hydrologic investigations of a potential nuclear waste disposal site at Yucca Mountain, southern Nevada: U.S. Geological Bulletin, v. 1790, p. 103–112.

Rosenbaum, J. G., 1986, Paleomagnetic directional dispersion produced by plastic deformation in a thick Miocene welded tuff, southern Nevada: Implications for welding temperatures: Journal of Geophysical Research, v. 91, p. 12,817–12,834.

Rosenbaum, J. G., Hudson, M. R., and Scott, R. B., 1991, Paleomagnetic constraints on the geometry and timing of deformation at Yucca Mountain, Nevada: Journal of Geophysical Research, v. 96, p. 1963–1979.

Rowan, M. G., and Kligfield, R., 1989, Cross section restoration and balancing as aid to seismic interpretation in extensional terranes: American Association of Petroleum Geologists Bulletin, v. 73, p. 955–966.

Sargent, K. A., McKay, E. J., and Burchfield, B. C., 1970, Geologic Map of the Striped Hills Quadrangle, Nye County, Nevada: U.S. Geological Survey Quadrangle Map GQ–882, 1:24,000.

Savage, J. C., 1998, Comment on detecting strain in the Yucca Mountain area, Nevada: Science, v. 282, p. 1007a.

Savage, J. C., Lisowski, M., Gross, W. K., King, N. E., and Svarc, J. L., 1994, Strain accumulation near Yucca Mountain, Nevada, 1983-1993: Journal of Geophysical Research, v. 99, p. 18,103–18,107.

Sawyer, D. R., Fleck, R. J., Lanphere, M. A., Warren, R. G., Broxton, D. E., and Hudson, M. R., 1994, Episodic caldera volcanism in the Miocene southwestern Nevada volcanic field: Revised stratigraphic framework, $^{40}Ar/^{39}Ar$ geochronology, and implications for magmatism and extension: Geological Society of America Bulletin, v. 106, p. 1304–1318.

Scott, R. B., 1990, Tectonic setting of the Yucca Mountain region, southwest Nevada: Geological Society of America Memoir, v. 176, p. 251–282.

Scott, R. B., and Bonk, J., 1984, Preliminary geologic map of Yucca Mountain, Nye County, Nevada, with geologic sections: U.S. Geological Survey Open-File Report 84-494, scale 1:12000.

Shelton, J. W., 1984, Listric normal faults: America Association of Petroleum Geologists Bulletin, v. 68, no. 7, p. 801–815.

Simonds, W. F., and 8 others, 1995, Map of fault activity of the Yucca Mountain area, Nye County, Nevada: U.S. Geological Survey Miscellaneous Investigations Series Map 1-2520, scale 1:24,000.

Smith, E. I., Feuerbach, D. L., Naumann, T. R. , and Faulds, J. E., 1990, The area of most recent volcanism near Yucca Mountain, Nevada: Implications for volcanic risk assessment: High-level radioactive waste management: Proceedings of the First Annual International Conference: La Grange, IL, American Nuclear Society, v. 1, p. 81–90.

Smith, E. I., Morikawa, S., and Sanchez, A., 1997, Summary of the activities of the center for volcanic and tectonic studies, University of Nevada, Las Vegas, for the period 1986–1996: Carson City, Nevada, The Nuclear Waste Projects Office, 43 p.

Snow, J. K., 1992, Large-magnitude Permian shortening and continental-margin tectonics in the southern Cordillera: Geological Society of America Bulletin, v. 104, p. 80–105.

Snyder, B. B., and Carr, W. J., 1982, Preliminary results of gravity investigations at Yucca Mountain and vicinity, southern Nye county, Nevada: U.S. Geological Survey Open-File Report 82-701, 36 p.

Snyder, D. B., and Carr, W. J., 1984, Interpretation of gravity data in a complex volcano-tectonic setting, southwestern Nevada: Journal of Geophysical Research, v. 89, p. 10,193–10,206.

Sonder, L. J., Jones, C. H., Salyards, S. L., and Murphy, K. M., 1994, Vertical axis rotations in the Las Vegas shear zone, southern Nevada: Paleomagnetic constraints on kinematics and dynamics of block rotations: Tectonics, v. 13, p. 769–788.

Stamatakos, J. A., and Ferrill, D. A., 1998, Strike-slip fault system in Amargosa Valley and Yucca Mountain, Nevada, by Schweickert, R. A., and Lahren, M. M., Comment: Tectonophysics, v. 294, p. 151–160.

Stamatakos, J. A., Kodama, K. P., and Pavlis, T. P., 1988, Paleomagnetism of Eocene plutonic rocks, Matanuska Valley, Alaska: Geology, v. 16, p. 618–622.

Stamatakos, J. A., Connor, C. B., and Martin, R. H., 1997, Quaternary basin evolution and basaltic magmatism of Crater Flat, Nevada, from detailed ground magnetic surveys of the Little Cones: Journal of Geology, v. 105, p. 319–330.

Stamatakos, J. A., Ferrill, D. A., and Spivey, K. H., 1998, Paleomagnetic constraints on the tectonic evolution of Bare Mountain, Nevada: Geological Society of America Bulletin, v. 110, p. 1530–1546.

Stewart, J. H., 1988, Tectonic of the Walker Lane belt, western Great Basin—Mesozoic and Cenozoic deformation in a zone of shear, *in* Ernst, W. G., ed., Metamorphism and crustal evolution of the western United States, Vol. VII: Prentice-Hall, Inc., p. 684–713.

Suppe, J., 1983, Geometry and kinematics of fault-bend folding: American Journal of Science, v. 283, p. 684–721.

Swadley, W. C, and Carr, W. J., 1987, Geologic map of the Quaternary and Tertiary deposits of the Big Dune Quadrangle, Nye County, Nevada, and Inyo County, California: U.S. Geological Survey Miscellaneous Investigations Series Map I–1767, scale 1:48,000.

Swadley, W. C., and Parrish, L. D., 1988, Surficial Geologic Map of the Bare Mountain Quadrangle, Nevada: U.S. Geological Survey Miscellaneous Investigations Series Map I-1826, scale 1:24,000.

Thordarson, W., 1983, Geohydrologic data and test results from Well J-13, Nevada Test Site, Nye County, Nevada: Water-Resources Investigation Report 83-4171, 32 p.

Trudgill, B., and Cartwright, J., 1994, Relay-ramp forms and normal-fault linkages, Canyonlands National Park, Utah: Geological Society of America Bulletin, v. 106, p. 1,143–1,157.

Turrin, D. B., Champion, D., and Fleck, R. J., 1991, $^{40}Ar/^{39}Ar$ Age of the Lathrop Wells Volcanic Center, Yucca Mountain, Nevada: Science, v. 253, p. 253–257.

U.S. Department of Energy, 1999, Geologic framework model (GFM3.1) analysis model report: U.S. Department of Energy, MDL-NBS-GS-000002, Rev. 00C (Draft Report).

U.S. Geological Survey, 1998, Probabilistic seismic hazard analyses for fault displacement and vibratory ground motion at Yucca Mountain, Nevada: Final Report, Wong, I.G., and Stepp, C., Report Coordinators: Oakland, CA, SP32IM3, WBS Number 1.2.3.2.8.3.6.

Van der Voo, R., Stamatakos, J. A., and Parés, J. M., 1997, Kinematic constraints on thrust-belt curvature from syndeformational magnetizations in the Lagos del Valle Syncline in the Cantabrian Arc, Spain: Journal of Geophysical Research, v. 102, p. 10,105–10,119.

Vaniman, D. T., Crowe, B. M., and Gladney, E. S., 1982, Petrology and geochemistry of Hawaiite lavas from Crater Flat, Nevada: Contributions to Mineralogy and Petrology, v. 80, p. 341–357.

Verrall, P., 1981, Structural interpretation with application to North Sea problems: Joint Association of Petroleum Exploration Courses (JAPEC), London, Course Notes No. 3.

Weiss, S. I., 1996, Hydrothermal activity, epithermal mineralization and regional extension in the southwestern Nevada volcanic field [Ph.D. dissert.]: Reno, Nevada, University of Nevada at Reno.

Wells, D. L., and Coppersmith, K. J., 1994, New empirical relationships among magnitude, rupture length, rupture width, rupture area, and surface displacement: Bulletin of the Seismological Society of America, v. 84, p. 974–1002.

Wernicke, B., Axen, G. A., and Snow, J. K., 1988, Basin and Range extensional tectonics at the latitude of Las Vegas, Nevada: Geological Society of America Bulletin, v. 100, p. 1738–1757.

Wernicke, B., and 8 others, 1998, Anomalous strain accumulation in the Yucca Mountain area, Nevada: Science, v. 279, p. 2,096–2,100.

Willemse, E. J. M., 1997, Segmented normal faults: Correspondence between three-dimensional mechanical models and field data: Journal of Geophysical Research, v. 102, p. 675–692.

Xiao, H., and Suppe, J., 1992, Origin of rollover: American Association of Petroleum Geologists Bulletin, v. 76, p. 509–529.

TABLE A1. SINGLE-GRAIN TOTAL FUSION ANALYSES OF 72696-5 FELDSPAR

WEIGHTED AVERAGE OF J FROM STANDARDS = 8.41634E-04 +/- 2.28489E-06

STANDARDS NAME	F1	F2	40*/39K	+/-	AGE	J	+/-
J function	0.00000E+00	0.00000E+00	1.85779E+01	5.04360E-02	2.79900E+07	8.41634E-04	2.28489E-06

72696-5 FRACTIONS

NAME	CUM 39K	F1	F2	40*/39K	+/-	AGE	+/-
F5A-5000 1223-	4.46078E-02	-2.32296E-03	1.10121E-02	6.73086E+00	4.48286E--01	1.01911E+07	6.76831E+05
F5-45 12-23-199	2.90978E-01	-1.82564E-03	2.36623E-03	5.90666E+00	2.47923E-01	8.94629E+06	3.74578E+05
F5-46 12-23-199	4.19620E-01	-1.70666E-03	3.38888E-03	5.83084E+00	2.02979E-01	8.83174E+06	3.06692E+05
F5-47 12-23-199	4.89031E-01	-1.66472E-03	1.11124E-02	6.36747E+00	2.58226E-01	9.64238E+06	3.89994E+05
F5-48 12-23-199	6.01241E-01	-1.51246E-03	5.24980E-03	6.07043E+00	2.55824E-01	9.19371E+06	3.86462E+05
F5-49 12-23-199	6.75508E-01	-1.56731E-03	8.11734E-03	5.76623E+00	3.21626E-01	8.73411E+06	4.85989E+05
F5-50 12-23-199	7.19332E-01	-1.69897E-03	1.04207E-02	5.01695E+00	3.86969E-01	7.60157E+06	5.85093E+05
F5-53 12-23-199	7.68309E-01	-1.89744E-03	2.22465E-03	5.41943E+00	6.17031E-01	8.21001E+06	9.32629E+05
F5-54 12-23-199	8.38322E-01	-1.72231E-03	7.15031E-03	5.92221E+00	3.78444E-01	8.96980E+06	5.71770E+05
F5-55 12-23-199	9.23342E-01	-1.76459E-03	5.60361E-03	6.49704E+00	2.91529E-01	9.83806E+06	4.40243E+05
F5-56 12-23-199	9.61374E-01	-1.49485E-03	1.03282E-02	5.58662E+00	4.23056E-01	8.46299E+06	6.39350E+05
F5-57 12-23-199	1.00000E+00	-1.77650E-03	1.39140E-02	6.13459E+00	4.60787E-01	9.29063E+06	6.96053E+05

NAME	TEMP	% ATMOS	37CA/39K	+/-	(40/36)S	+/-	VOL ATMOS 40/G
F5A-5000 12-23-	5.00000E+03	7.46336E+01	3.58387E+00	2.05748E-02	3.95934E+02	8.93761E+00	9.28045E-09
F5-45 12-23-199	5.00000E+03	8.94242E+01	2.81659E+00	6.83144E-03	3.30447E+02	1.63835E+00	1.29270E-07
F5-46 12-23-199	5.00000E+03	8.68083E+01	2.63303E+00	6.29979E-03	3.40405E+02	1.79779E+00	5.18552E-08
F5-47 12-23-199	5.00000E+03	6.99332E+01	2.56832E+00	1.13251E-02	4.22546E+02	7.34911E+00	1.07995E-08
F5-48 12-23-199	5.00000E+03	8.08173E+01	2.33342E+00	8.38105E-03	3.65640E+02	3.65102E+00	3.01484E-08
F5-49 12-23-199	5.00000E+03	7.61903E+01	2.41804E+00	1.23178E-02	3.87845E+02	6.74368E+00	1.43964E-08
F5-50 12-23-199	5.00000E+03	7.60676E+01	2.62117E+00	1.62559E-02	3.88470E+02	9.40711E+00	7.34124E-09
F5-53 12-23-199	5.00000E+03	9.06905E+01	2.92736E+00	2.51776E-02	3.25833E+02	3.80278E+00	2.71649E-08
F5-54 12-23-199	5.00000E+03	7.89066E+01	2.65718E+00	7.84990E-03	3.74494E+02	6.38999E+00	1.62948E-08
F5-55 12-23-199	5.00000E+03	8.08187E+01	2.72241E+00	1.03536E-02	3.65633E+02	3.88518E+00	2.44505E-08
F5-56 12-23-199	5.00000E+03	7.20246E+01	2.30626E+00	1.87877E-02	4.10277E+02	1.20327E+01	5.74691E-09
F5-57 12-23-199	5.00000E+03	6.76587E+01	2.74079E+00	2.26616E-02	4.36751E+02	1.56374E+01	5.20760E-09

Notes: Integrated results: mass of sample = 0.0184g; (40/36)S =s 351.225 ±1.08849; $^{37}CA/^{39}K$ = 2.68151 ± .0028738; F1 = -1.73808E-03; F2 = 4.55603E-03; total atmospheric ^{40}Ar volume = 3.31956E-07 CCNTP/g; Total ^{39}K volume = 1.05058E-08 CCNTP/g; $^{40*}/^{39}K$ = 5.95867E+00 ± 9.80888E-02; age = 9.02488E+06 ± 1.50194E+05 years

TABLE A2. $^{40}Ar/^{39}Ar$ AGE SPECTRA AND STEP-WISE HEATING ISOCHRON RESULTS FOR MIOCENE BASALTS IN SOUTHERN CRATER FLAT, NEVADA

Sample	Total gas age (Ma)	Plateau $\%^{39}Ar$	Plateau MSWD*	Plateau age (Ma)	n†	Isochon $40Ar/^{36}Ar$	Isochon age (MA)	Isochon MSWD*
DFCF1 (fine)	11.12±0.18	89	0.89	11.24±0.18	17	295.8±5.4	11.19±0.26	0.74
DFCF1 (coarse)	10.97±0.16	87	0.58	11.17±0.14	ND	ND	ND	ND
DFCF2 (fine)	11.10±0.26	94	0.65	11.31±0.24	16	292.4±9.0	11.29±0.24	0.78
DFCF2 (fine)	10.89±0.14	85	0.84	11.12±0.12	ND	ND	ND	ND
Mean	**11.0±0.38**			**11.21±0.35§**			**11.24±0.35§**	

Note: **Fine (100–300 microns) and coarse(1–2 mm) refer to companion analyses for each sample based on grain-size fraction of the crushed rock material. The two sets of runs were ganged together to form the single isochron results for each sample. All errors are reported as 2 sigma.**

***Denotes the mean square weighted deviate and a measure of the linearity of the isochron line.**

†Denotes the number of points in the isochron plot.

§ Error is square root of sum of squares of sample errors.

TABLE A3. GEOCHEMICAL ANALYSES FOR MIOCENE BASALT IN THE CRATER FLAT BASIN. MAJOR ELEMENT ABUNDANCES IN WEIGHT PERCENT NORMALIZED TO 100% VOLATILE FREE WITH ORIGINAL LOSS ON IGNITION AND TOTALS SHOWN. TRACE ELEMENT ABUNDANCES IN MG/G.

Sample #	42396-2	2795-3	72396-1	VH-2-1193	1σ	Analysis
Unit:	Solitario	WCH	WCH	VH-2	(%)	type
SiO_2	50.8	50.4	50.3	51.6	1	XRF
TiO_2	2.17	1.56	1.52	1.60	3	XRF
Al_2O_3	16.3	16.1	16.6	17.1	1	XRF
Fe_2O_3*	11.17	9.94	10.11	9.37	2	XRF
MnO	0.17	0.15	0.15	0.12	1	XRF
MgO	4.66	7.37	7.13	5.98	1	XRF
CaO	8.12	8.93	9.32	8.72	1	XRF
Na_2O	3.64	3.24	2.93	3.18	2	XRF
K_2O	2.05	1.61	1.31	1.65	1	XRF
P_2O_5	0.95	0.71	0.61	0.71	1	XRF
L.O.I.	0.14	0.24	0.19	2.24	ND	ND
Total	100.05	100.38	100.08	99.90	ND	ND
Mg#	49.3	63.3	62.2	59.8		
Rb	42	26	23	28	10	XRF
Ba	1460	1090	1107	1197	3	INA
Sr	1060	1020	980	940	4	INA
Cs	0.7	0.7	0.6	2.2	10	INA
Sc	21.2	21.2	23.5	21.0	1	INA
V	247	198	202	194	3	XRF
Co	29.3	34.6	36.5	29.2	1	INA
Ni	15	124	86	77	7	XRF
Cr	9	254	211	166	3	INA
Cu	20	37	37	35	7	XRF
Zn	110	91	92	93	14	XRF
La	74.0	51.0	48.6	57.2	1	INA
Ce	154	105	98	115	1	INA
Nd	70	45	45	51	8	INA
Sm	12.4	8.6	8.1	9.1	1	INA
Eu	3.14	2.38	2.35	2.49	1	INA
Tb	1.26	0.93	0.88	0.94	3	INA
Yb	2.81	2.18	2.01	2.21	2	INA
Lu	0.41	0.31	0.31	0.33	3	INA
Zr	334	234	216	260	3	XRF
Hf	7.3	5.1	4.8	5.6	2	INA
Y	37	27	24	28	8	XRF
Nb	20	19	12	15	15	XRF
Ta	0.77	0.75	0.53	0.65	4	INA
Th	7.89	6.33	6.82	6.03	1	INA
U	1.0	1.4	1.4	1.3	10	INA

TABLE A4. PALEOMAGNETIC RESULTS FROM MIOCENE BASALT AND MEGABRECCIA, SOUTHERN CRATER FLAT, NEVADA

			In-Situ		Stratigraphic					
Site	DD/D	n/N	Dec	Inc	Dec	Inc	κ	α_{95}	R	ΔR
11.2-Ma Basalt										
TCFb1	220/13	4/8	189.7	-35.9	183.3	-46.8	66.1	11.4	6.4	13.8
TCFb2	040/10	8/8	197.6	-57.9	202.2	-48.5	37.5	9.4	25.2	11.4
TCFb4	040/10	7/8	186.5	-57.6	193.3	-49.2	84.3	6.6	16.3	8.6
TCFb4	040/10	8/8	181.3	-60.9	189.9	-52.6	79.3	6.0	12.9	8.4
TCFb5	075/22	8/8	146.7	-65.8	194.7	-63.4	93.8	5.8	17.7	10.7
TCFb6	077/32	8/8	140.3	-40.9	172.0	-47.3	25.9	11.1	-5.0	13.4
Mean (*in-situ*)		6/6	174.0	-55.4			19.1	15.7	-3.0	23.0
Mean (stratigraphic)		**6/6**			**188.8**	**-51.7**	**78.4**	**7.6**	**12.3**	**10.3**
Megabreccia										
TCFmbl1	040/10	6/15	345.8	54.6	356.7	49.4	17.5	18.7	-0.3	23.9
TCFmbl1	040/10	5/13	152.7	-63.2	168.1	-58.1	13.6	21.5	-8.9	35.3
TCFmbl1	040/10	3/9	344.1	63.0	357.2	56.5	37.9	20.3	0.2	31.3
TCFmbl1	040/10	6/8	180.2	-60.7	189.0	-52.5	12.8	19.4	12.0	26.6
TCFmbl1	040/10	7/8	359.9	56.0	007.5	47.8	48.1	8.8	10.5	10.9
Mean (*in-situ*)		5/5	349.1	59.5			132.7	6.7	-7.9	10.1
Mean (stratigraphic)		**5/5**			**359.9**	**52.9**	**132.7**	**6.7**	**2.9**	**9.0**

Notes: **DD and D are the *in-situ* dip direction and dip of bedding at each site. n is the number of samples that produced ChRM directions, and N is the number of samples from each site demagnetize. Dec and Inc are the declination and inclination of the site mean direction, in degrees. κ is the Fisher (1953) precision parameter and α_{95} is the 95% confidence region about the mean value. R is the vertical axis rotation, positive clockwise. ΔR is the 95% confidence interval around R following Demarest (1983). Bold values indicate the best estimate of the grand mean direction**

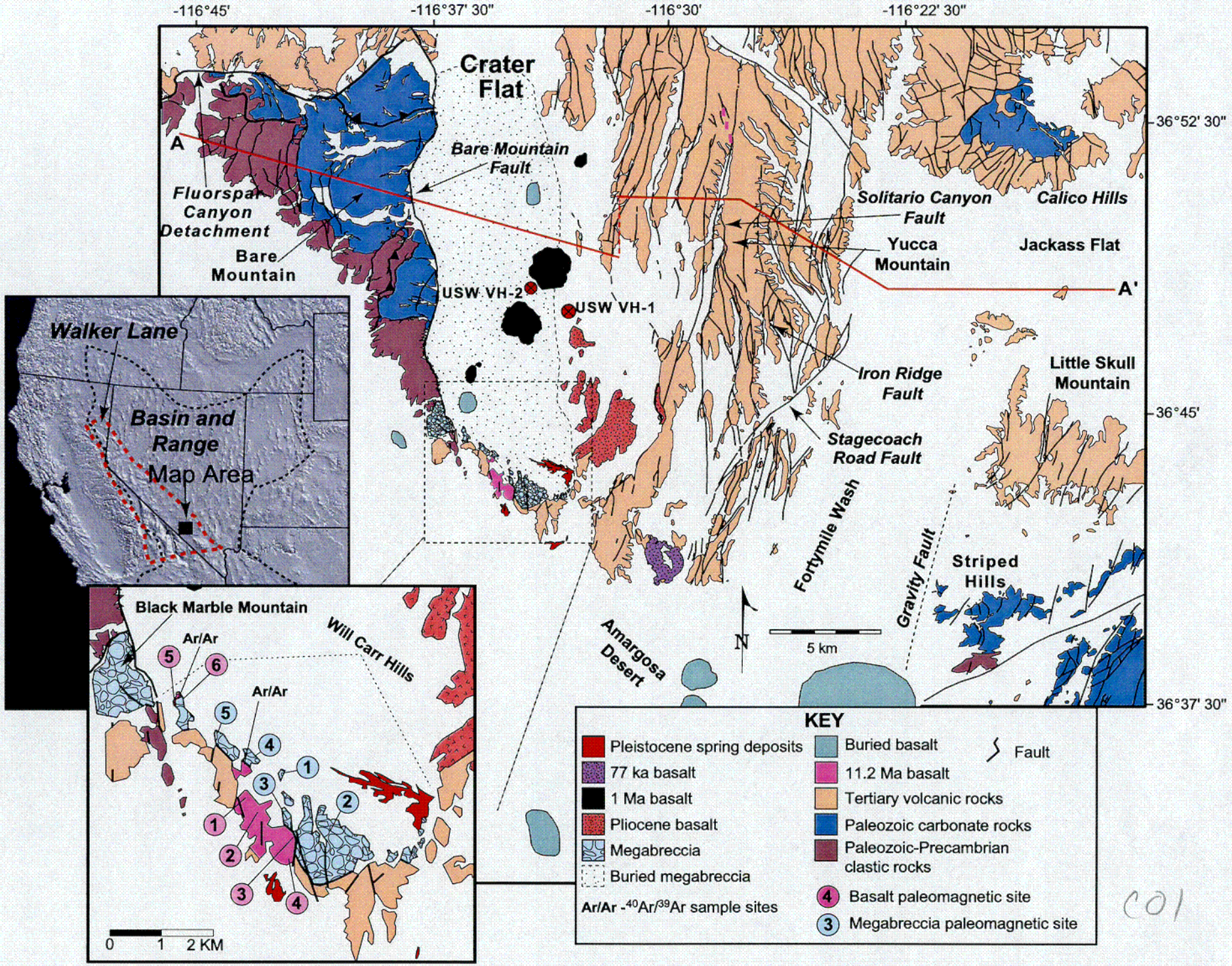

C01

Stamatakos et al., Composite 13 Ma.... Figure 1

Precambrian and Paleozoic Rocks Bare Mountain[1]

Mississippian		
	Eleana Fm.	
Devonian	Fluorspar Canyon Fm. / Rocks of Tarantula Canyon	
	Lone Mountain Dolomite	
Silurian	Roberts Mountain Fm.	
Ordovician	Ely Springs Dolomite	
	Eureka Quartzite	
	Pogonip Group	Antelope Valley Fm.
		Ninemile Fm.
		Goodwin Limestone
Cambrian	Nopah Fm.	
	Bonanza King Fm.	
	Carrara Fm.	
	Zabriskie Quartzite	
	Wood Canyon Fm.	
	Stirling Quartzite	
Late Proterozoic		

Miocene Silicic Volcanic Rocks[2]

Thirsty Canyon Group	9.2 Ma 9.4 Ma
Timber Mountain Group	11.45 Ma 12.5 Ma
Paintbrush Group	12.7 Ma 12.8 Ma
Calico Hills Fm.	12.9 Ma
Wahmonie Fm.	13.0 Ma
Crater Flat Group	
Belted Range Group	13.5 Ma
Lithic Ridge Tuff	14.0 Ma
Older Miocene-Oligocene Tuffs	

Neogene and Quarternary Rocks

Quarternary Sedimentary and Volcanic Deposits	Spring Deposits	18 ±1 ka[3] 30 ±1 ka[3] 45 ±1 ka[3]
	Basalt Lathrop Wells	77 ±5 ka[4]
	Spring Deposits	70 ka-1.4 Ma[5]
	Basalt Crater Flat	1.0 ±0.2 Ma[6,7]
Neogene Sedimentary Deposits	Basalt Crater Flat	3.7 ±0.2 Ma[6]
	Carbonate Megabreccia	< 11.45 Ma
	Basalt Crater Flat	11.1 ±0.3 Ma[8,9]
	Basalt Soltario Canyon	11.7 ±0.3Ma[10]
	Carbonate Megabreccia	< 12.7 Ma > 11.7 Ma

Stamatakos et al., Composite 13 Ma....
Figure 2

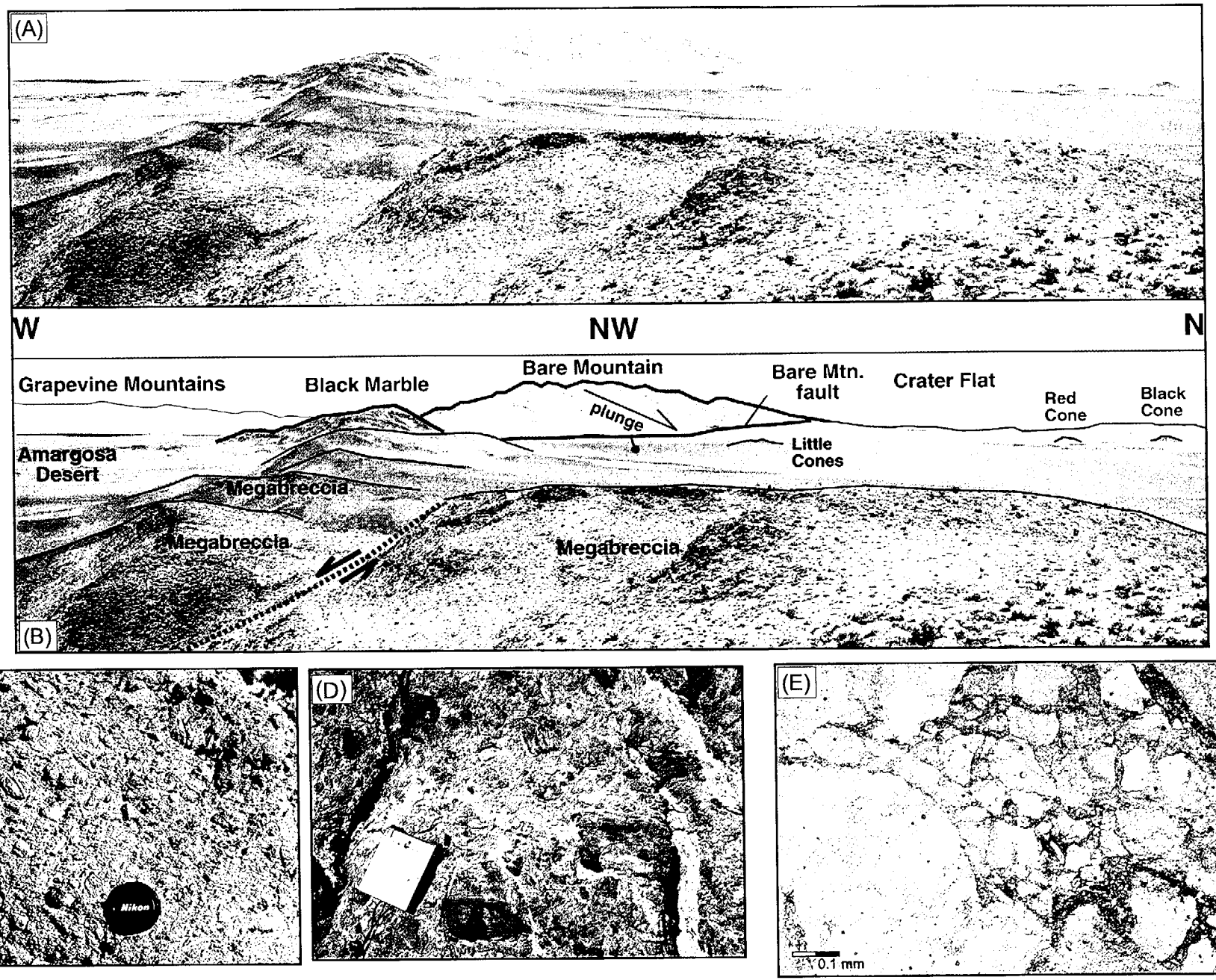

Stamatakos et al., Composite 13 Ma....
Figure 3

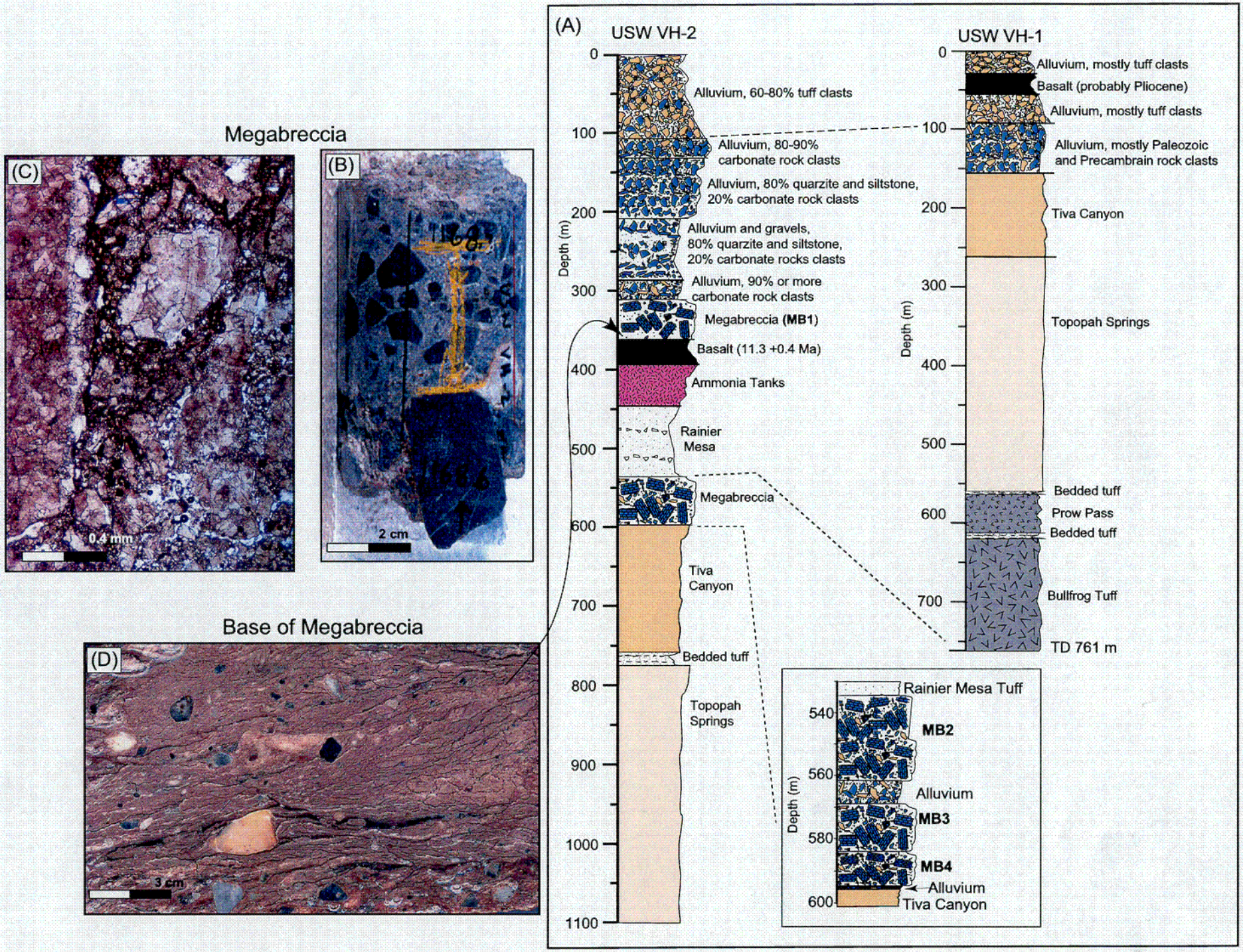

C02

Stamatakos et al., Composite 13 Ma.... Figure 4

(A) Complete Bouguer Anomaly (gravity) map

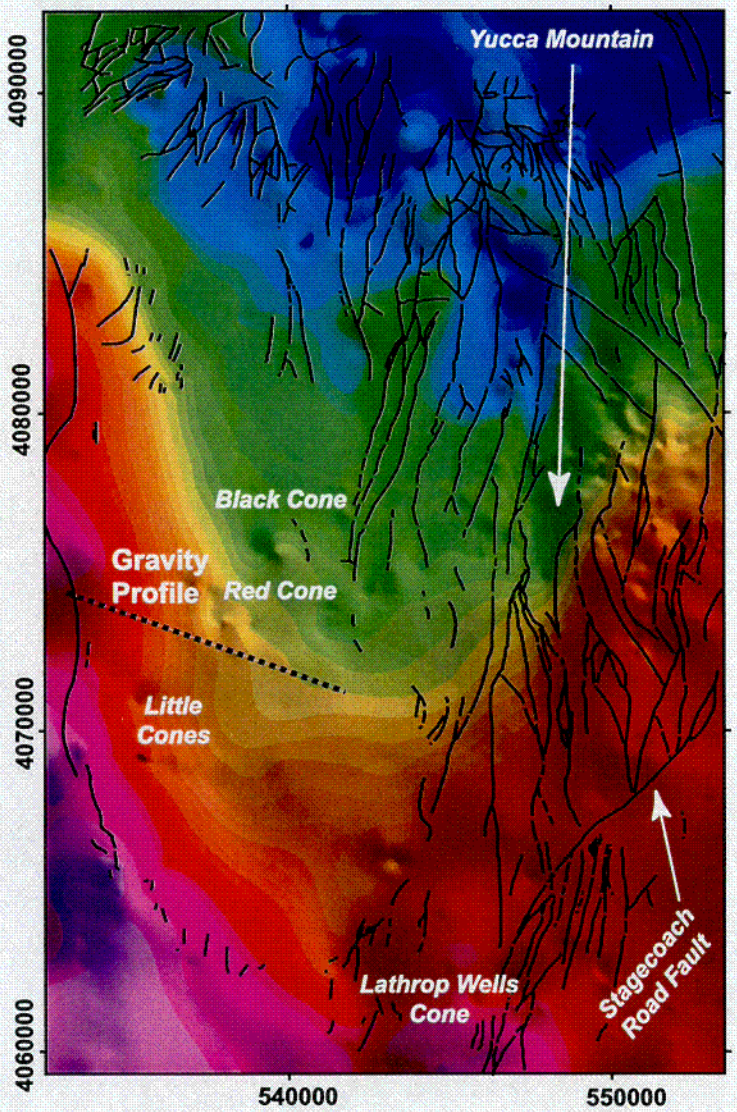

(B) Aeromagnetic anomaly map

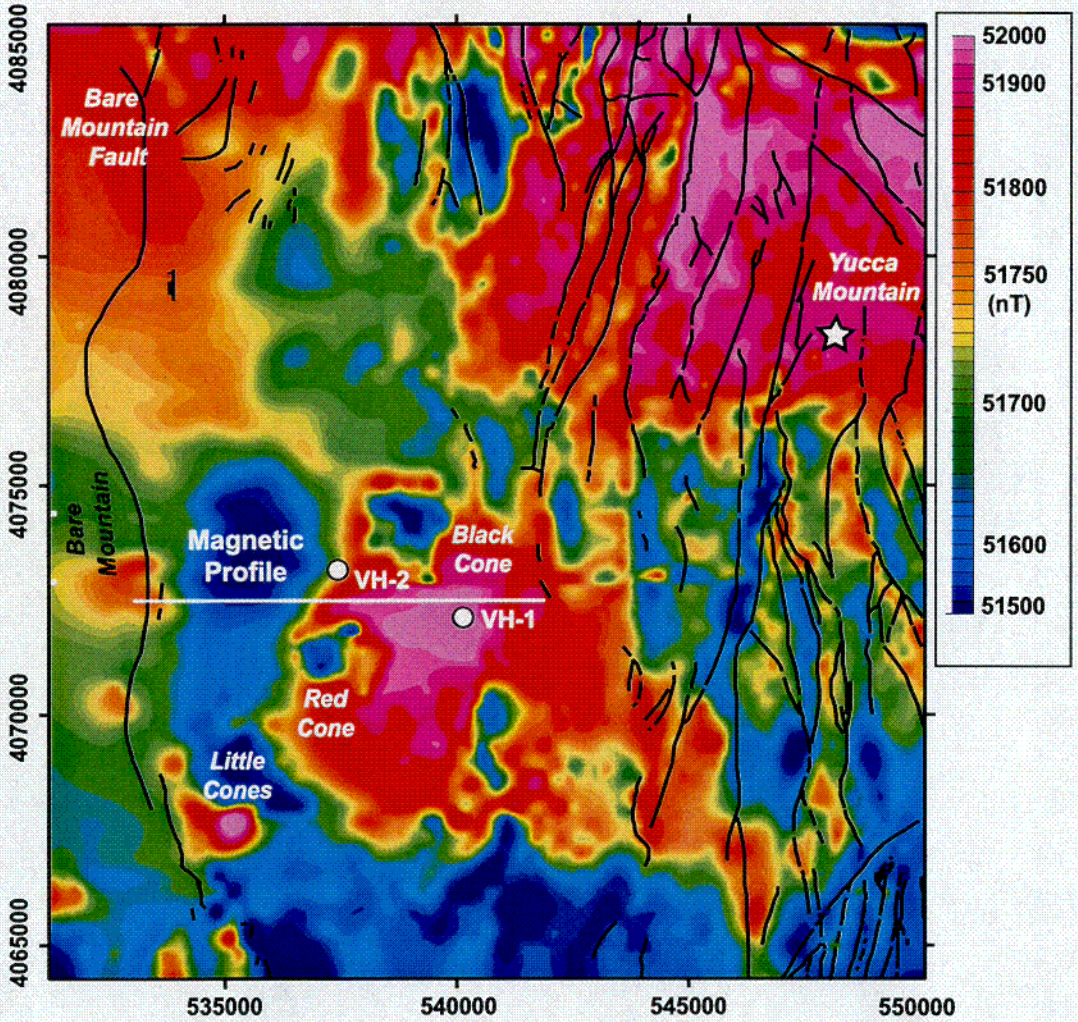

C03

Stamatakos et al., Composite 13 Ma....
Figure 5

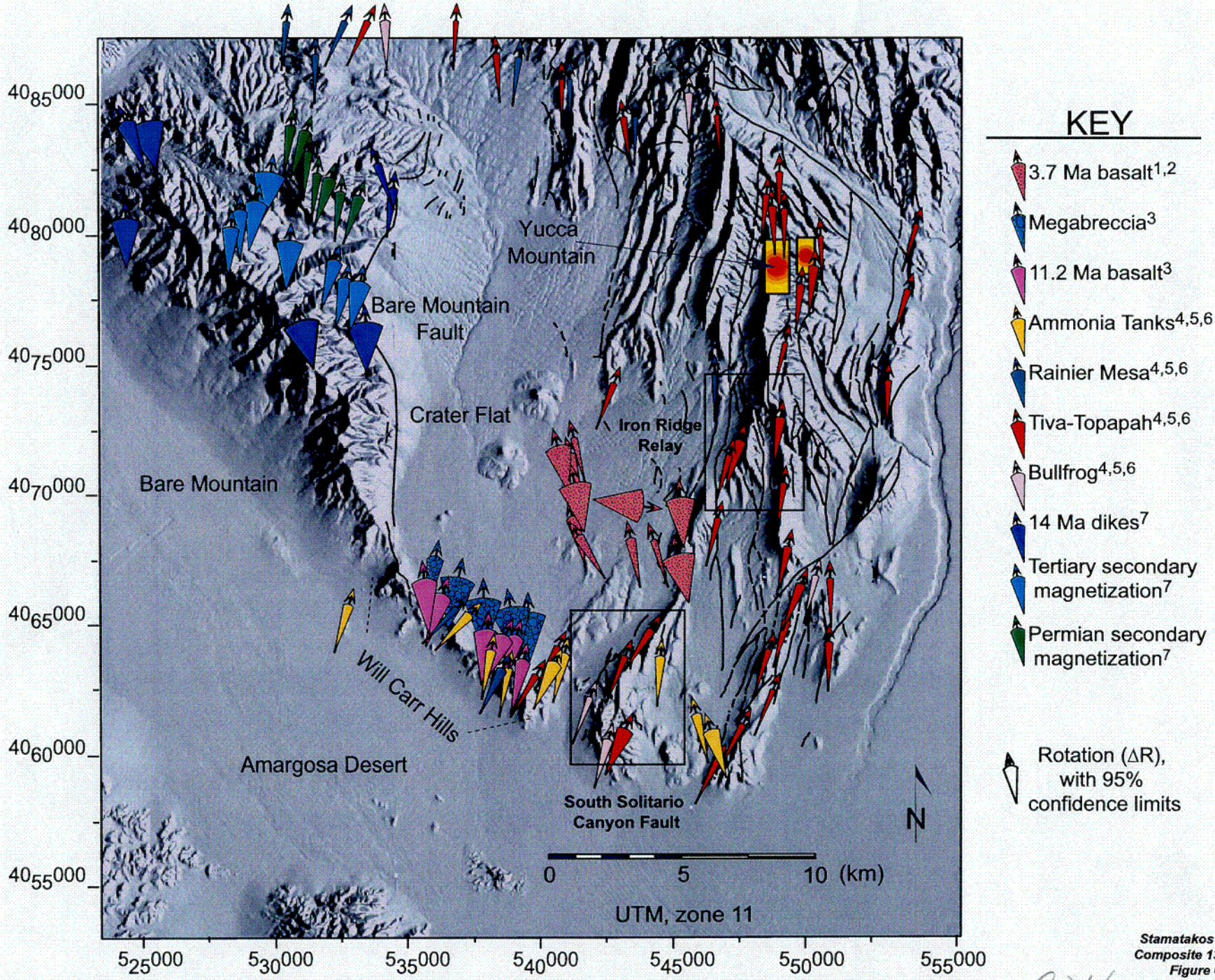

Stamatakos et al., Composite 13 Ma.... Figure 6

C04

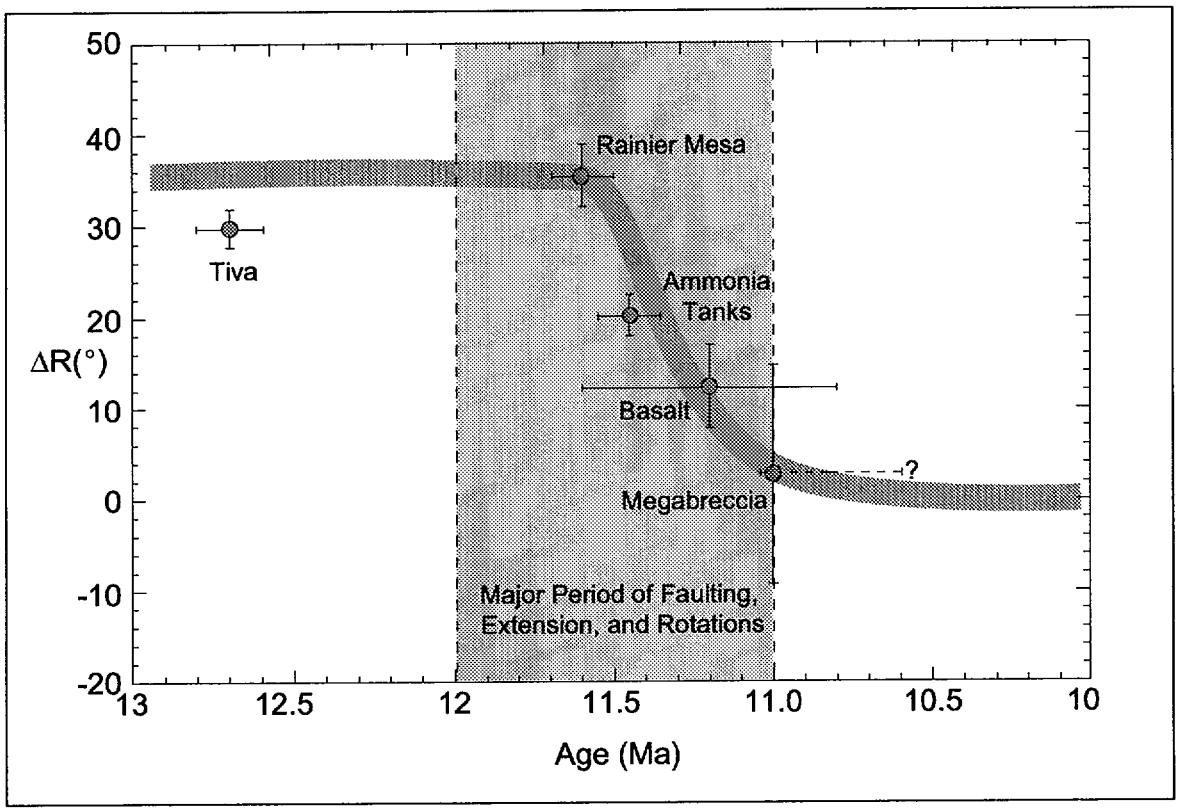

Stamatakos et al.,
Composite 13 Ma....
Figure 7

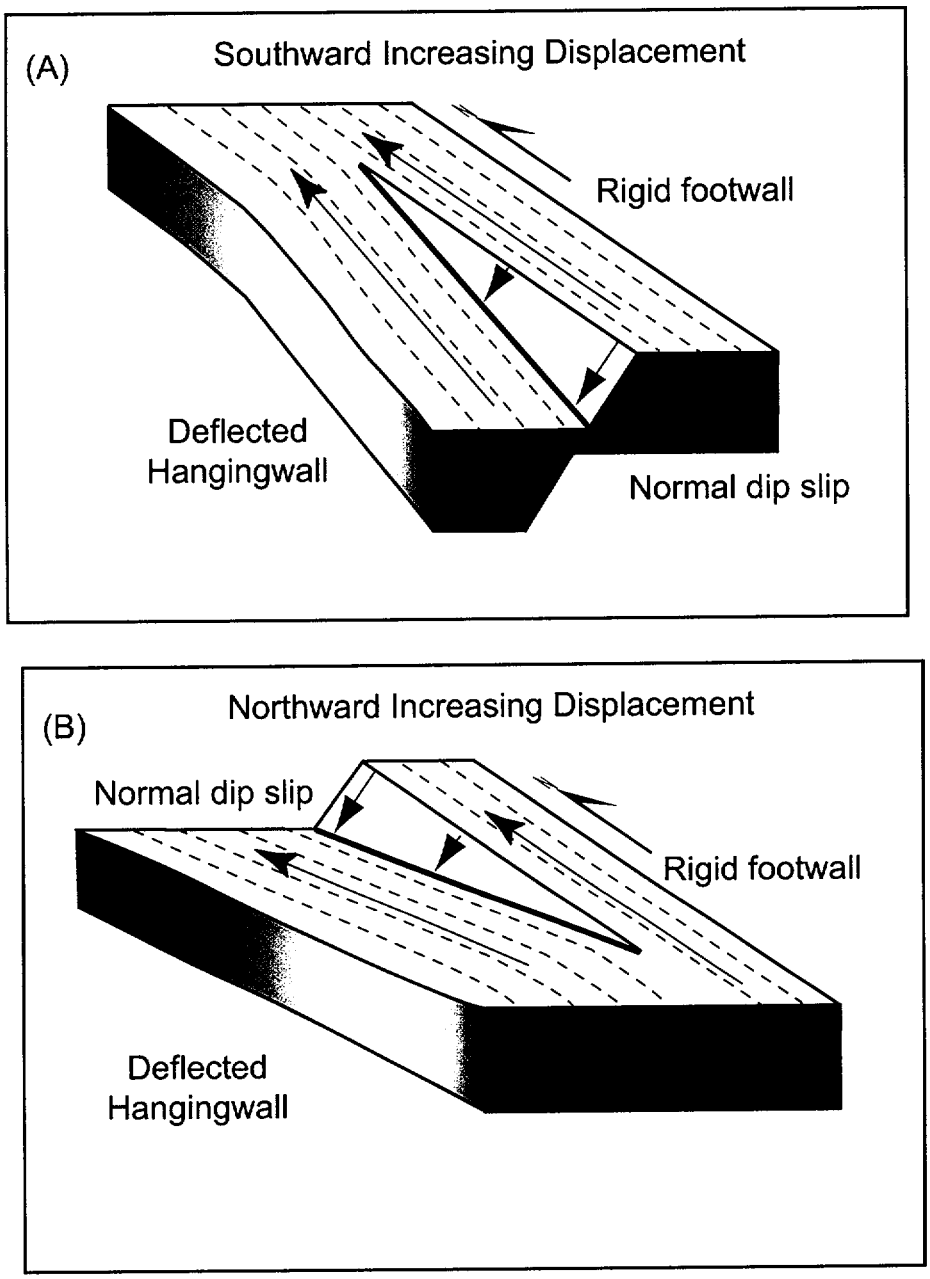

Stamatakos et al.,
Composite 13 Ma...
Figure 8

(A) Iron Ridge Relay

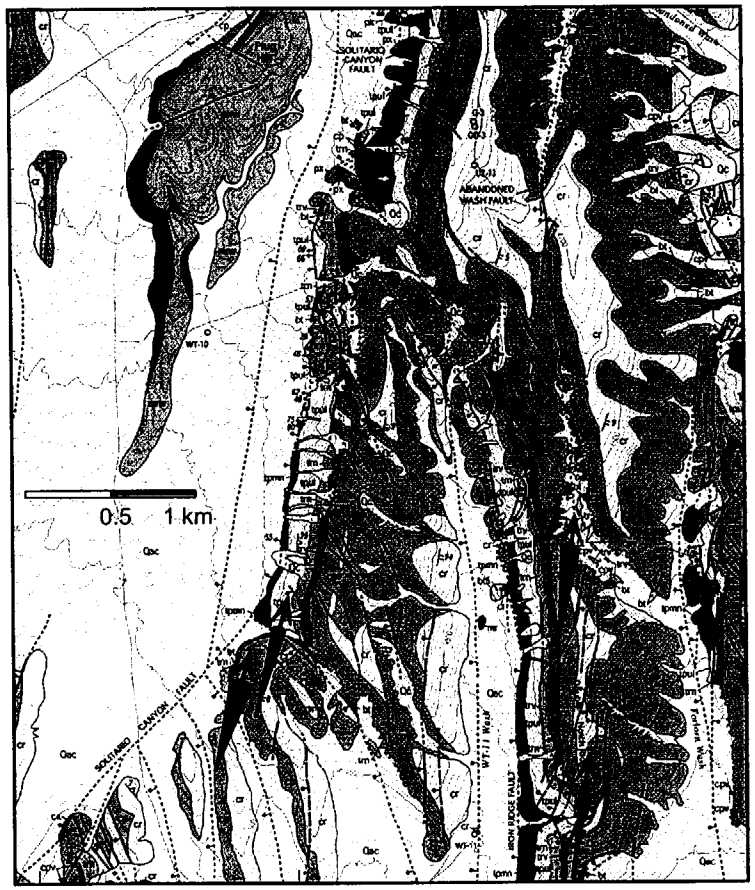

(B) South Solitario Canyon Relay

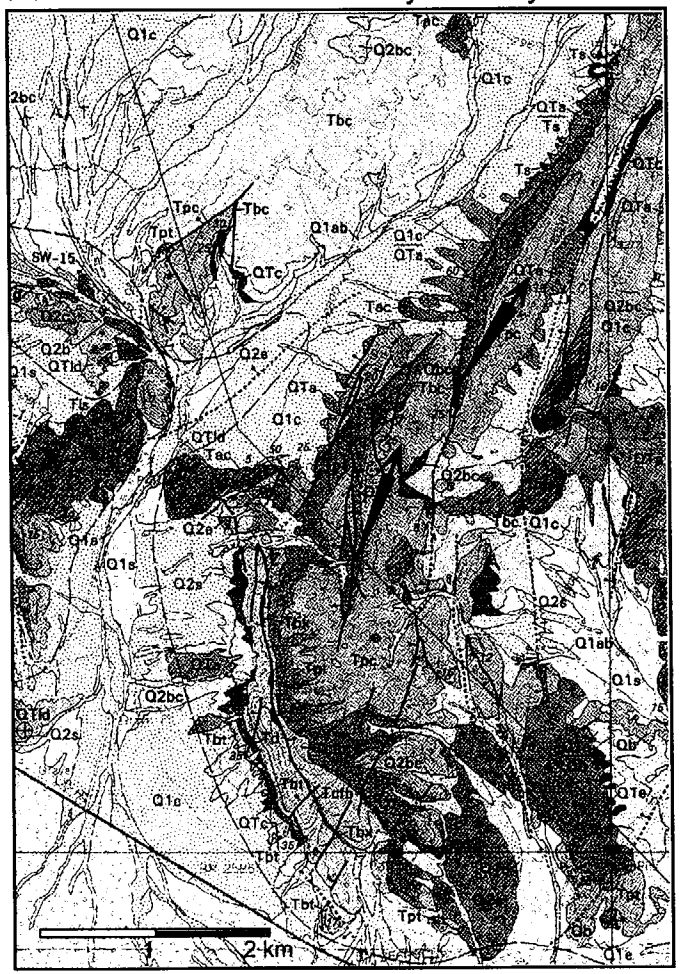

Stamatakos et al.,
Composite 13 Ma...
Figure 9

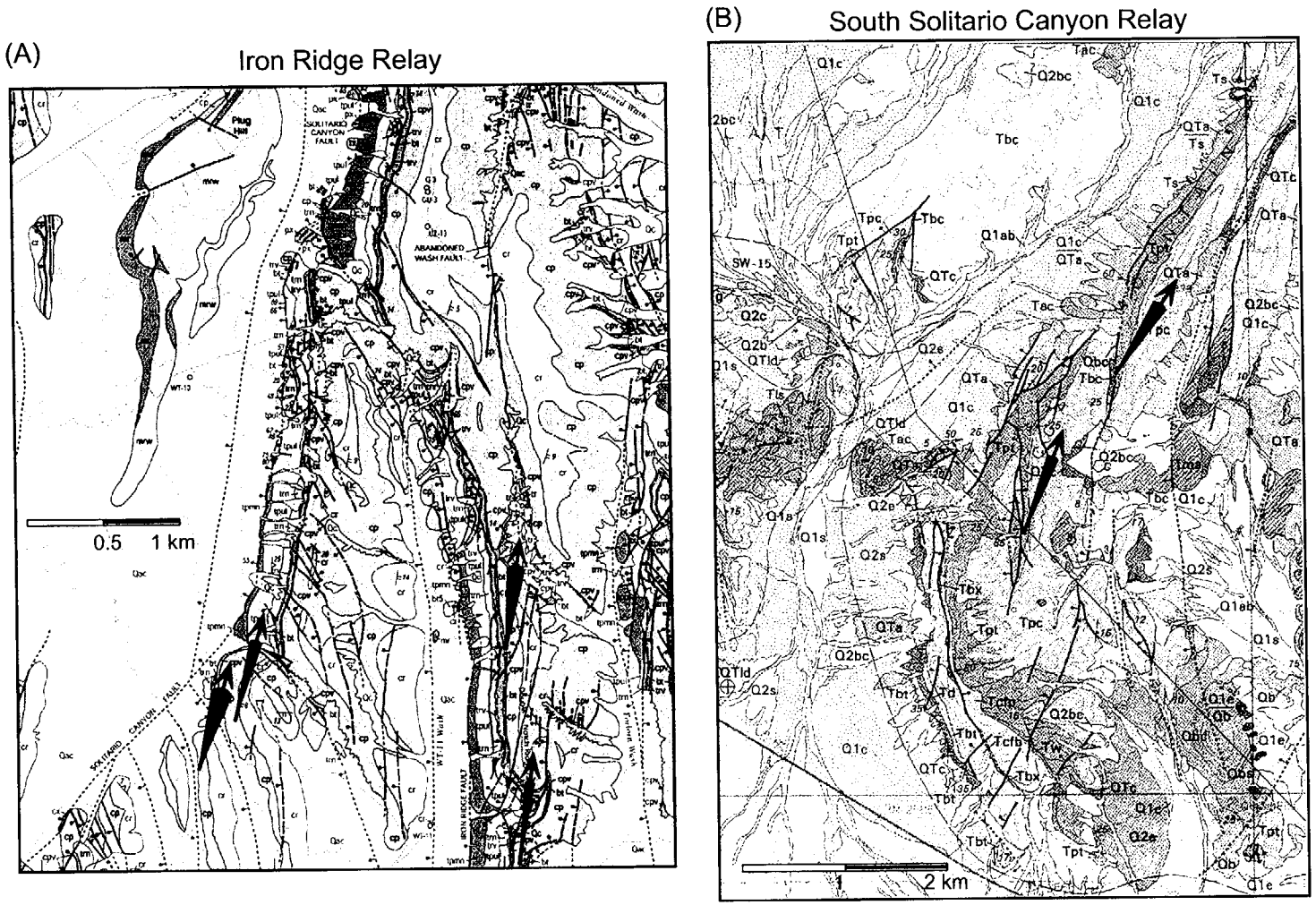

Stamatakos et al.,
Composite 13 Ma...
Figure 9

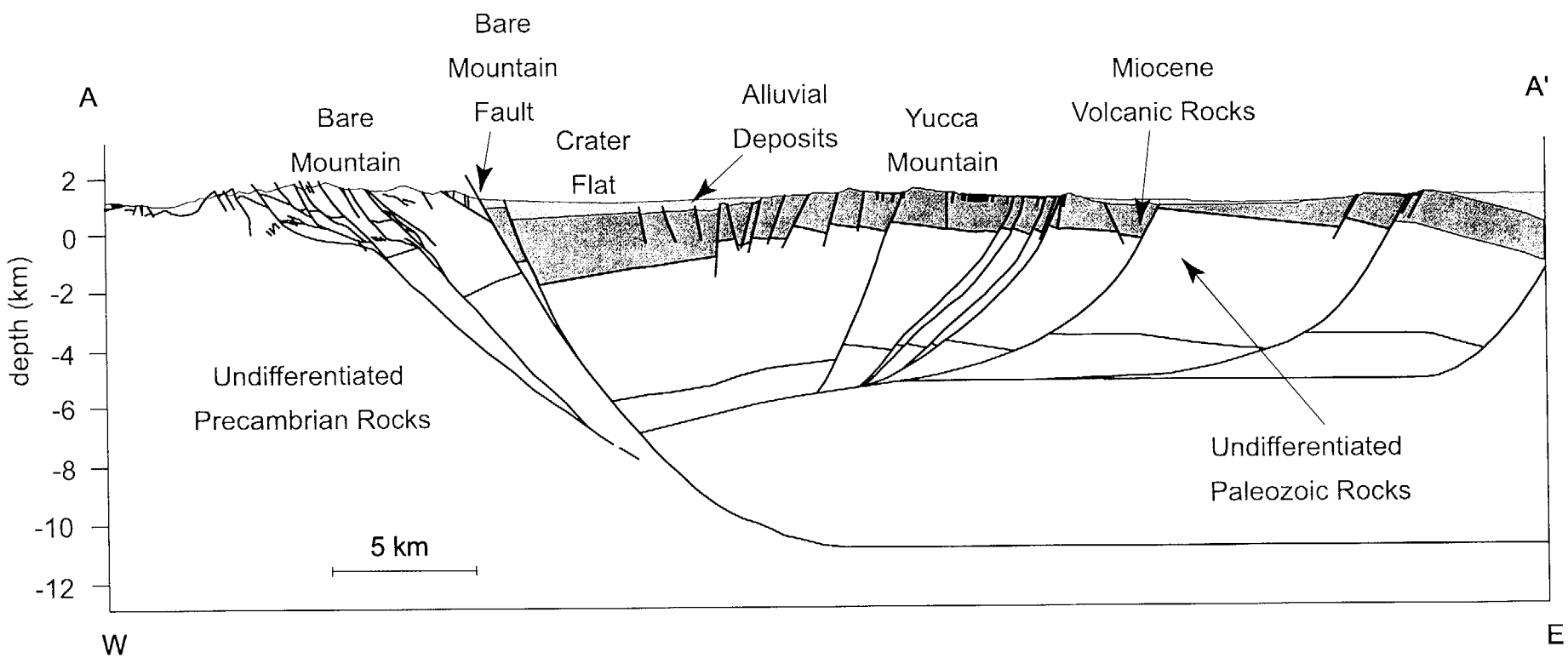

Stamatakos et al.,
Composite 13 Ma...
Figure 10

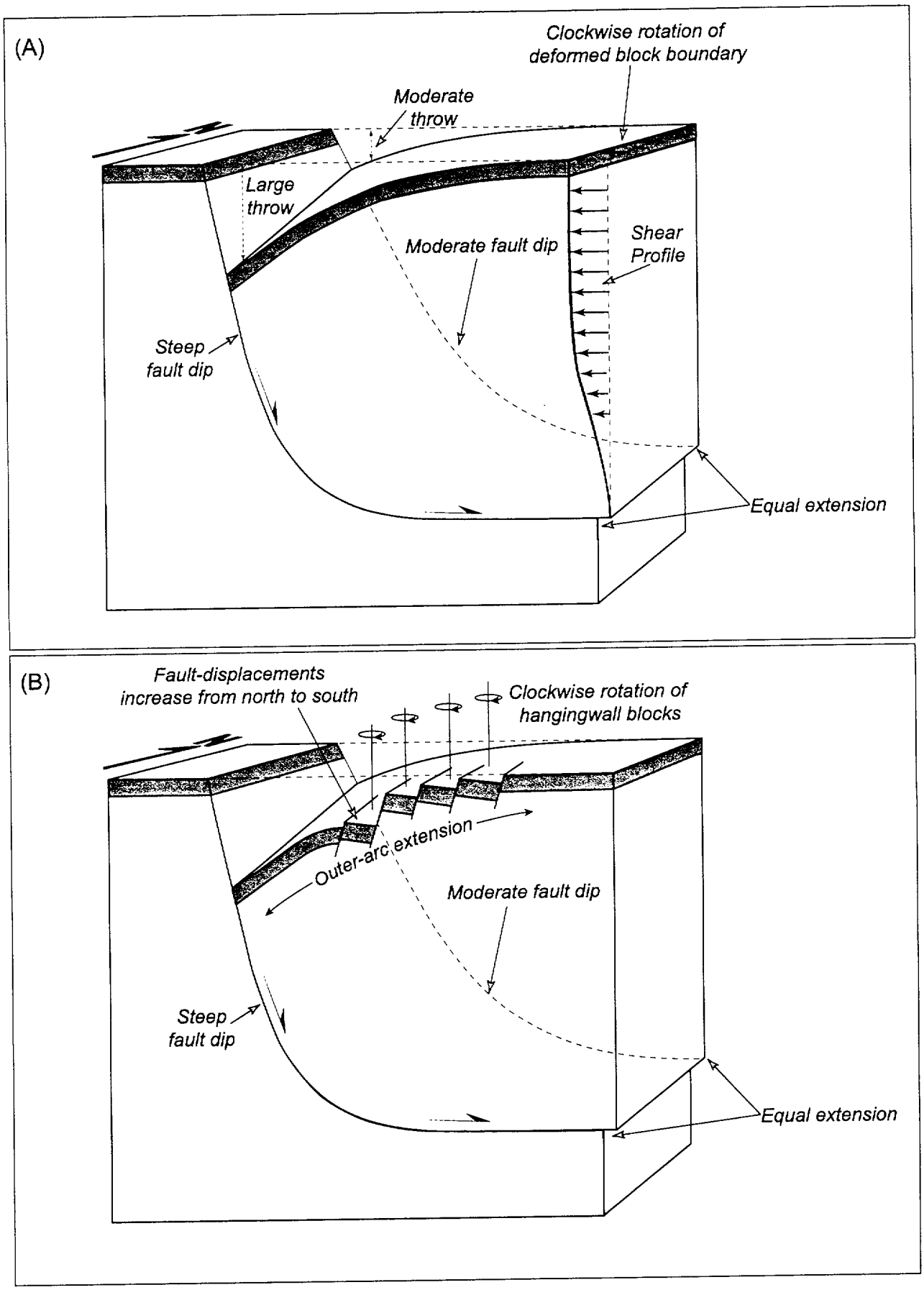

Stamatakos et al.,
Composite 13 Ma...
Figure 11

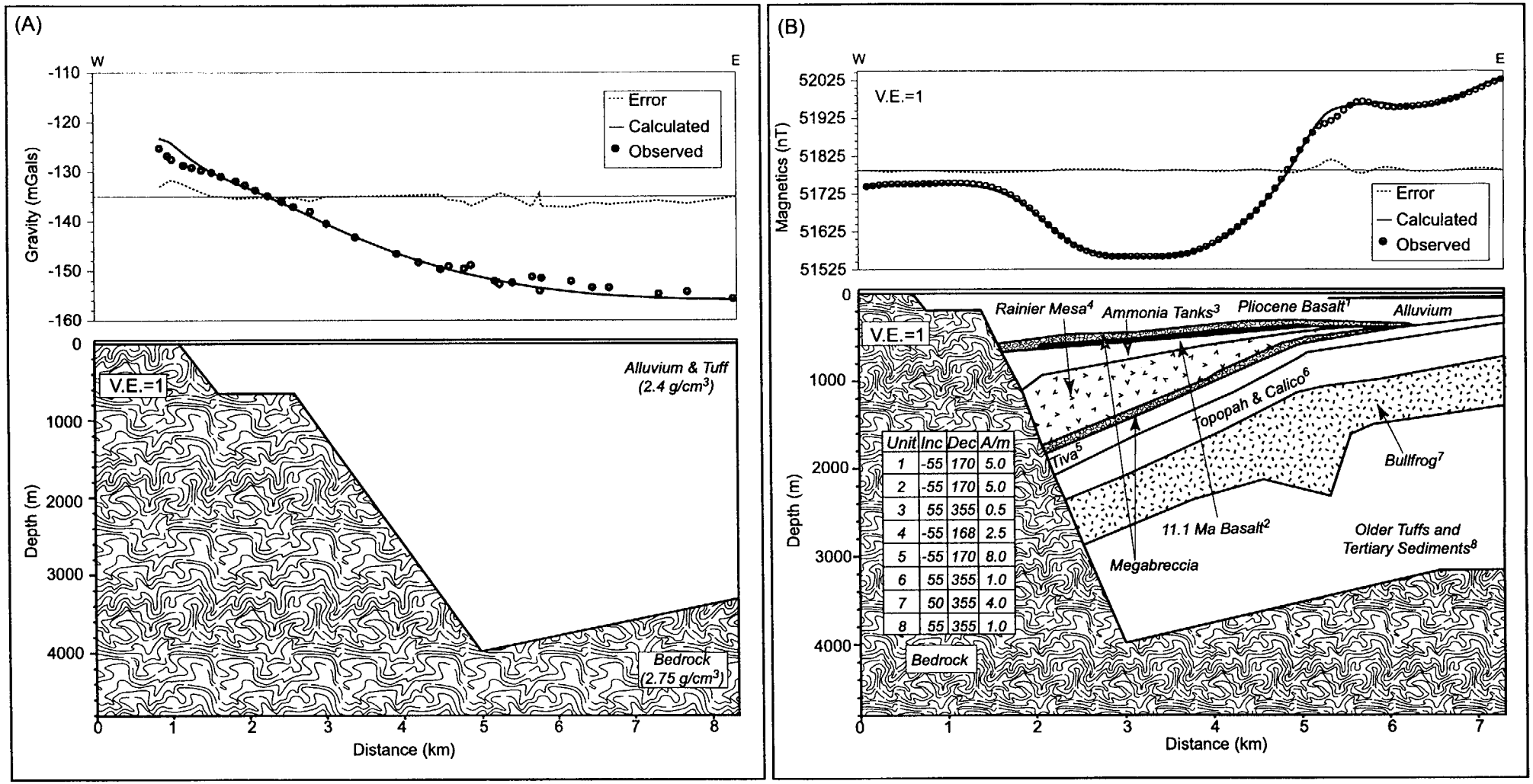

Stamatakos et al.,
Composite 13 Ma....
Figure 12

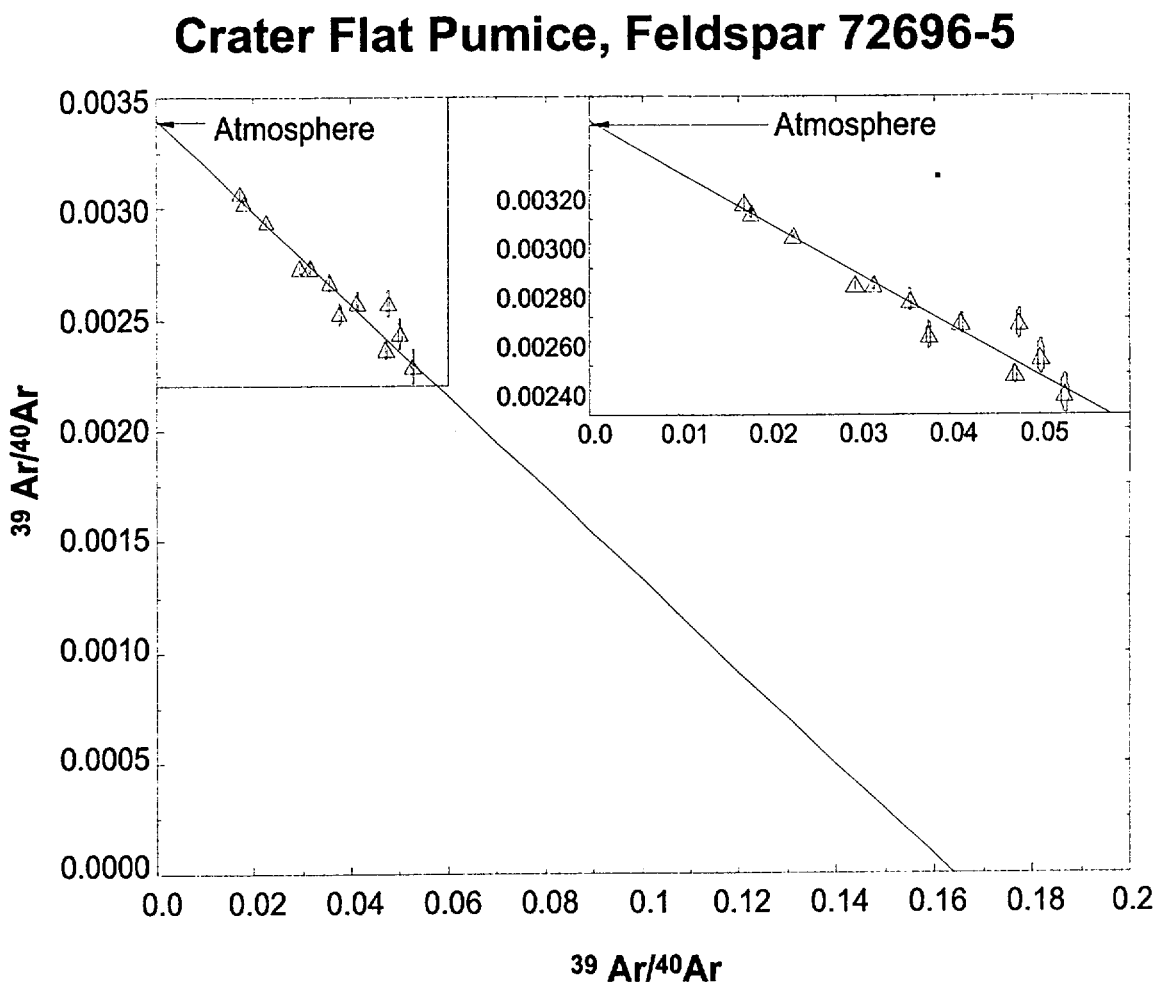

Stamatakos et al.,
13 Ma Composite...
Figure A1

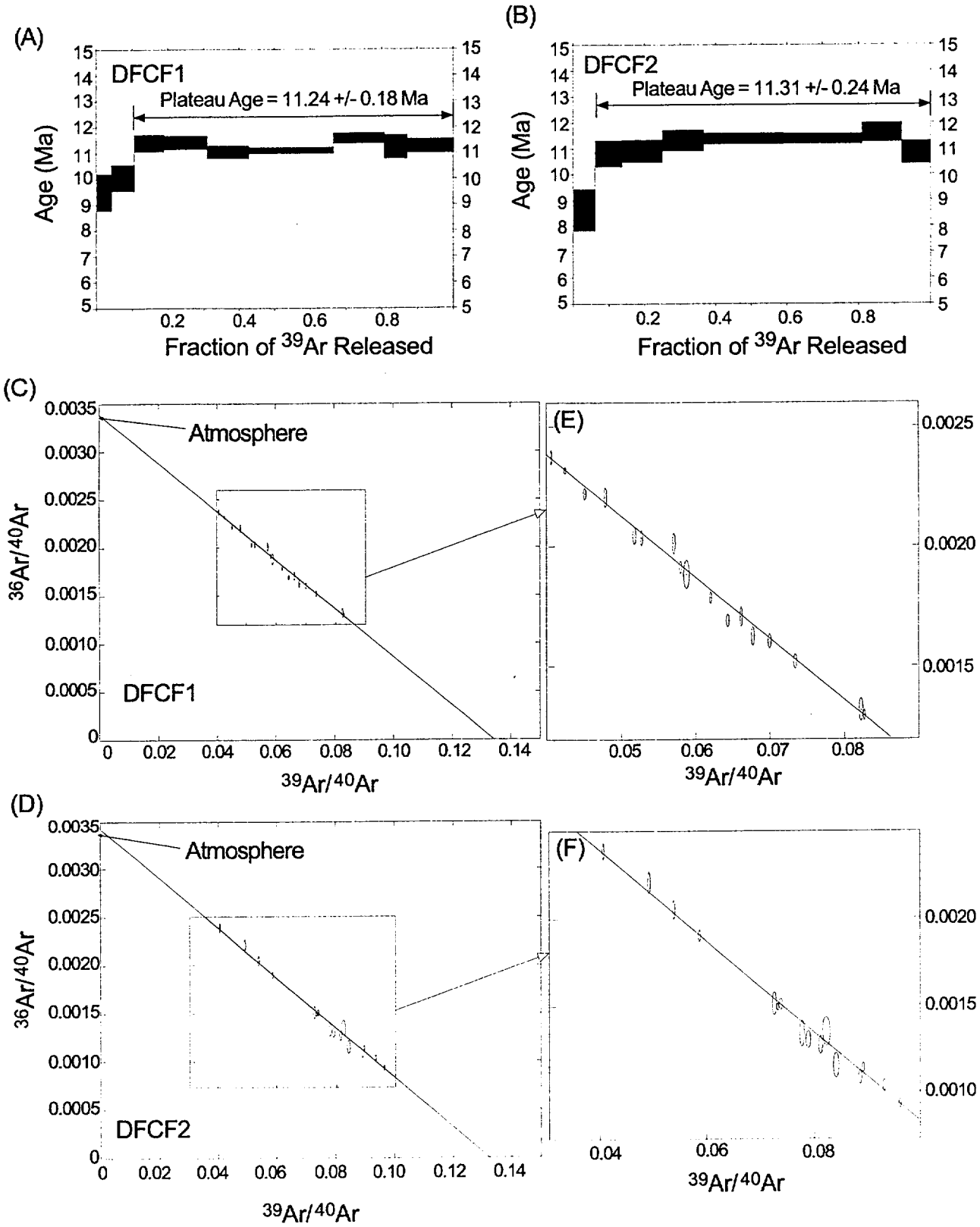

Stamatakos et al.,
13 Ma Composite...
Figure A2

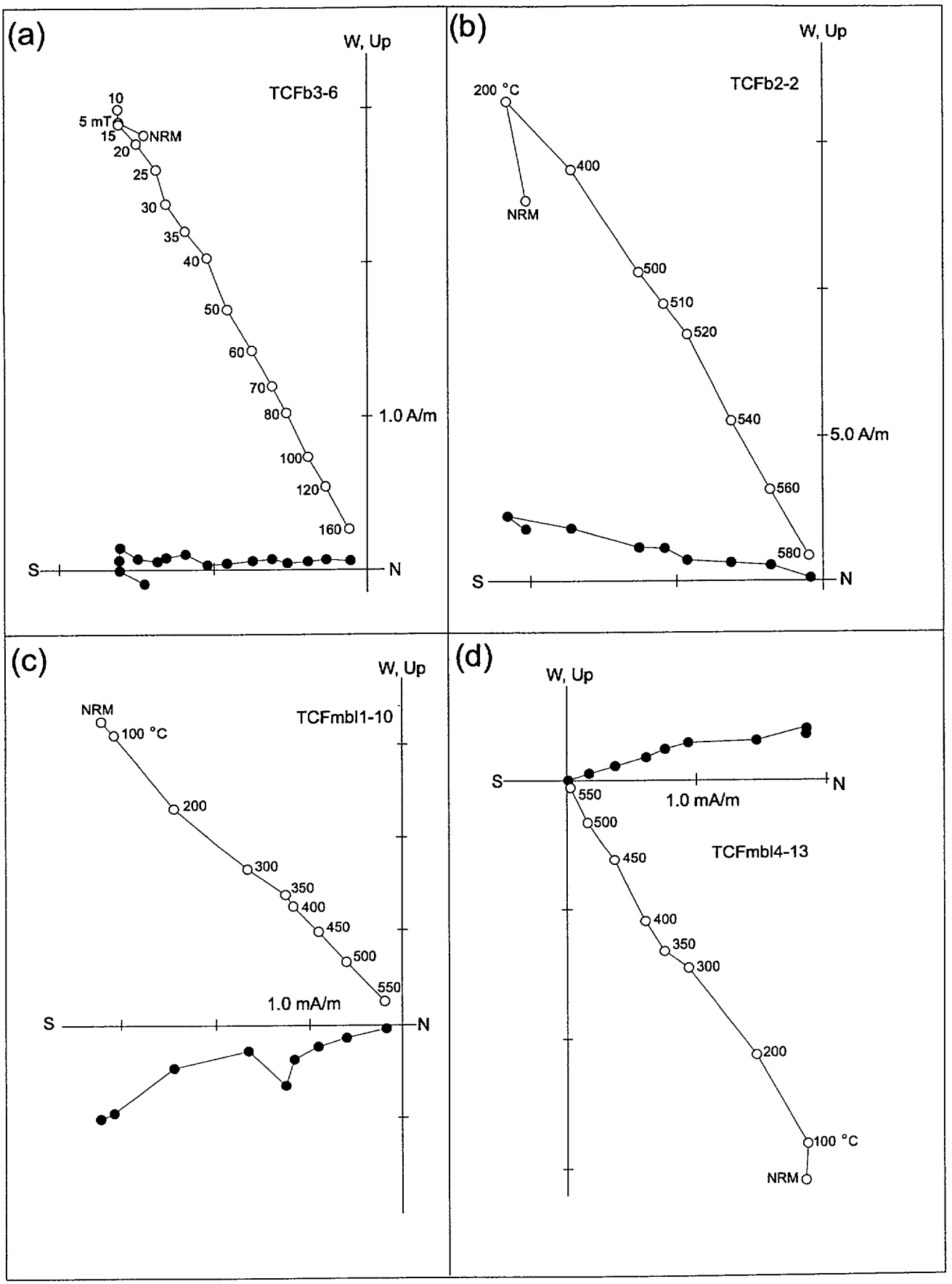

Stamatakos et al.,
13 Ma Composite...
Figure A3

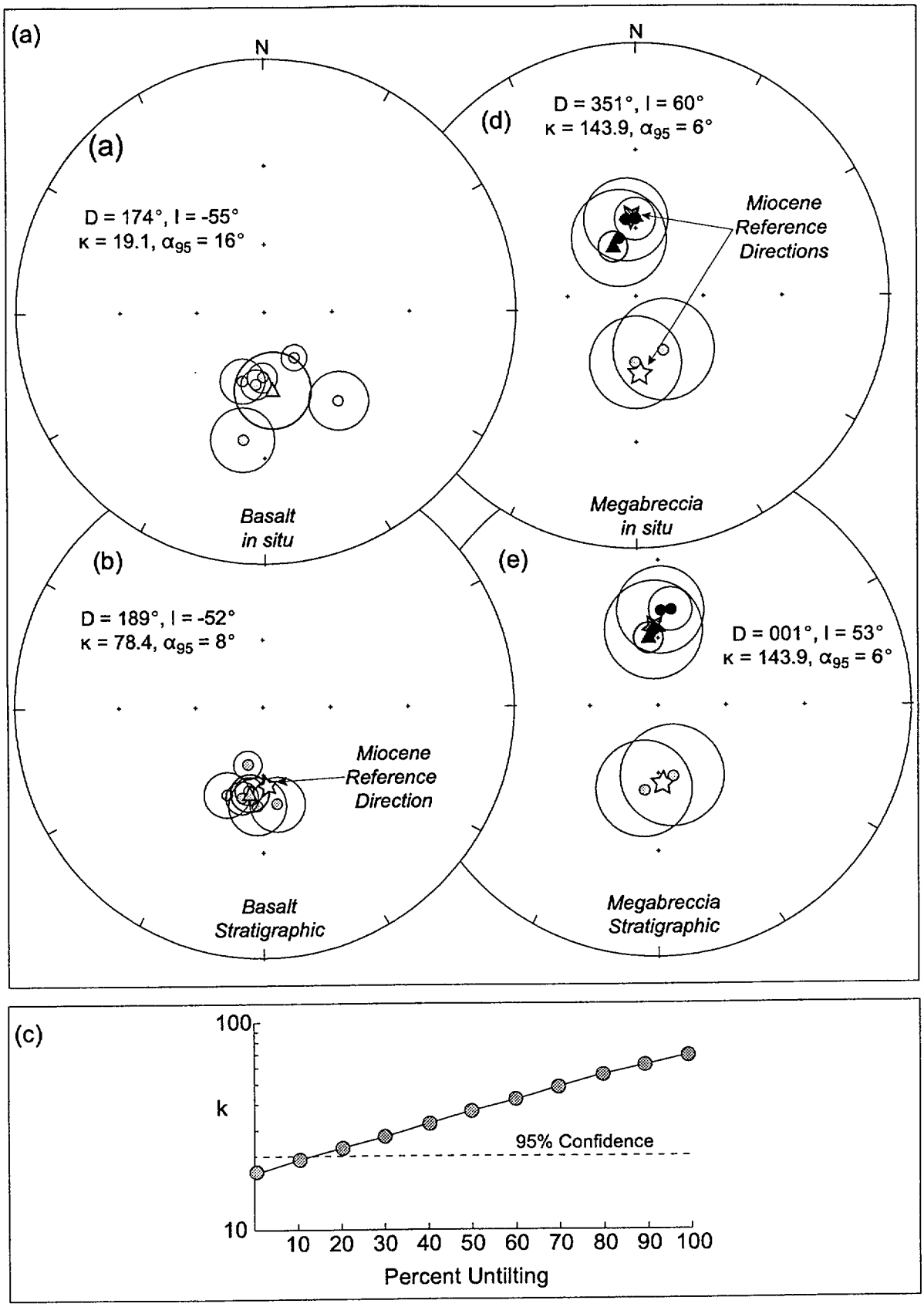

Stamatakos et al.,
13 Ma Composite...
Figure A4